bioRxiv preprint doi: https://doi.org/10.1101/677054; this version posted June 19, 2019. The copyright holder for this preprint (which was not certified by peer review) is the author/funder, who has granted bioRxiv a license to display the preprint in perpetuity. It is made available under aCC-BY 4.0 International license.

Depletion of Ric-8B leads to reduced mTORC2 activity

Maíra H. Nagai[1], Luciana M. Gutiyama[1#], Victor P. S. Xavier[1], Cleiton F. Machado[1], Alice H. Reis[2], Elisa R. Donnard[3], Pedro A. F. Galante[3], Jose G. Abreu[2], William T. Festuccia[4] and Bettina Malnic[1*]

[1]Department of Biochemistry, University of São Paulo, Av. Prof. Lineu Prestes, 748, CEP 05508-000, São Paulo, SP, Brazil.

[2] Institute of Biomedical Sciences, Federal University of Rio de Janeiro, Rio de Janeiro, RJ, Brazil.

[3] Centro de Oncologia Molecular, Hospital Sírio-Libanês, São Paulo, Brazil.

[4]Department of Physiology and Biophysics, Institute of Biomedical Sciences, University of São Paulo, São Paulo, SP, Brazil.

#Current address: Centro de Transplante de Medula Óssea, Instituto Nacional do Câncer, Rio de Janeiro, RJ, Brazil.

* Corresponding author: Bettina Malnic

E-mail: bmalnic@iq.usp.br

bioRxiv preprint doi: https://doi.org/10.1101/677054; this version posted June 19, 2019. The copyright holder for this preprint (which was not certified by peer review) is the author/funder, who has granted bioRxiv a license to display the preprint in perpetuity. It is made available under aCC-BY 4.0 International license.

Abstract

mTOR, a serine/threonine protein kinase that is involved in a series of critical cellular processes, can be found in two functionally distinct complexes, mTORC1 and mTORC2. In contrast to mTORC1, little is known about the mechanisms that regulate mTORC2. Here we show that mTORC2 activity is reduced in mice with a hypomorphic mutation of the Ric-8B gene. Ric-8B is a highly conserved protein that acts as a non-canonical guanine nucleotide exchange factor (GEF) for heterotrimeric Gαs/olf type subunits. We found that Ric-8B hypomorph embryos are smaller than their wild type littermates, fail to close the neural tube in the cephalic region and die during mid-embryogenesis. Comparative transcriptome analysis revealed that signaling pathways involving GPCRs and G proteins are dysregulated in the Ric-8B mutant embryos. Interestingly, this analysis also revealed an unexpected impairment of the mTOR signaling pathway. Phosphorylation of Akt at Ser 473 is downregulated in the Ric-8B mutant embryos, indicating a decreased activity of mTORC2. In contrast, phosphorylation of S6, a downstream target of mTORC1, is unaltered. Knockdown of the endogenous Ric-8B gene in HEK293T cells leads to reduced phosphorylation levels of Akt at Ser 473, but not of S6, further supporting the selective involvement of Ric-8B in mTORC2 activity. Our results reveal a crucial role for Ric-8B in development and provide novel insights into the signals that regulate mTORC2 activity.

Author Summary

bioRxiv preprint doi: https://doi.org/10.1101/677054; this version posted June 19, 2019. The copyright holder for this preprint (which was not certified by peer review) is the author/funder, who has granted bioRxiv a license to display the preprint in perpetuity. It is made available under aCC-BY 4.0 International license.

Gene inactivation in mice can be used to identify genes that are involved in important biological processes and that may contribute to disease. By using this approach, we found that the Ric-8B gene is essential for embryogenesis and for the normal development of the nervous system. Ric-8B mutant mouse embryos are smaller than their wild type littermates and show neural tube defects at the cranial region. This approach also allowed us to identify the biological pathways that are involved in the observed phenotypes, the G protein and mTORC2 signaling pathways. mTORC2 plays particular important roles also in the adult brain, and has been implicated in neurological disorders. Ric-8B is highly conserved in mammals, including humans. Our mutant mice provide a model to study the complex molecular and cellular processes underlying the interplay between Ric-8B and mTORC2 in neuronal function.

bioRxiv preprint doi: https://doi.org/10.1101/677054; this version posted June 19, 2019. The copyright holder for this preprint (which was not certified by peer review) is the author/funder, who has granted bioRxiv a license to display the preprint in perpetuity. It is made available under aCC-BY 4.0 International license.

Introduction

Ric-8B (resistant to inhibitors of cholinesterase 8B) is a highly conserved protein which interacts with Gαs class subunits from heterotrimeric G proteins [1,2]. *In vitro*, Ric-8B can work as a guanine nucleotide exchange factor (GEF) for both Gαs and Gαolf [1,3]. While Gαs is ubiquitously expressed, Gαolf is restrictedly expressed in the olfactory neurons and in a few regions of the brain, such as the striatum [4-6]. Ric-8B expression in adult mice is highly predominant in the same tissues where Gαolf is expressed indicating that these two proteins are functional partners *in vivo* [2]. Consistent with the role of a GEF, Ric-8B is able to amplify odorant receptor signaling or dopamine receptor signaling through Gαolf in cultured cells [2,7-9]. Also, a series of studies indicate that Ric-8B regulates Gα protein abundance in the cells, and suggest that Ric-8B may serve as a chaperone that promotes Gα protein stability and the formation of functional G protein complexes [7,8,10-13].

In addition to the full-length Ric-8B, an alternatively spliced version of Ric-8B lacking exon 9, denominated Ric-8BΔ9, is also highly expressed in the olfactory epithelium. Differently from full-length Ric-8B, Ric-8BΔ9 does not bind to Gαs and does not show GEF activity, or does it very inefficiently [2,3]. Studies have shown that both, Ric-8B and Ric-8BΔ9 are able to interact with the different Gγ subunit types, Gγ13, Gγ7 and Gγ8 [10]. Chan and colleagues showed that Ric-8BΔ9, but not full-length Ric-8B, can bind Gβ1γ2 [3]. These results suggest that besides

bioRxiv preprint doi: https://doi.org/10.1101/677054; this version posted June 19, 2019. The copyright holder for this preprint (which was not certified by peer review) is the author/funder, who has granted bioRxiv a license to display the preprint in perpetuity. It is made available under aCC-BY 4.0 International license.

92 acting on the Gαs subunits, the Ric-8B proteins may also play a role in Gβγ
93 signaling.

94 Despite the restricted pattern of expression in adult mice, previous studies have
95 shown that complete knockout of the Ric-8B gene results in mice that are not
96 viable and that die early during embryogenesis (between E4 and E8.5) [7]. Here
97 we investigated the physiological roles of Ric-8B during development using a gene
98 trapped allele of Ric-8B that shows reduced levels of Ric-8B expression. We found
99 that the Ric-8B mutant embryos are small, fail to close the neural tube at the
100 cephalic region and die around E10.5. In the embryo, Ric-8B gene expression is
101 predominant in the nervous system, more specifically in the neural folds in the
102 cephalic region and in the ventral region of the neural tube. Increased apoptosis is
103 observed in the region of the cranial defects in the Ric-8B mutant embryos.
104 Comparative transcriptome analysis revealed that mTOR signaling is impaired in
105 the Ric-8B mutant embryos. mTOR is a serine/threonine protein kinase that acts as
106 the catalytic core of two distinct complexes: mTORC1 and mTORC2. mTORC1
107 mainly controls cell growth and metabolism, promotes protein synthesis and is the
108 best characterized complex to date [14,15]. mTORC2, on the other hand, has been
109 implicated in the regulation of cytoskeletal organization, cell survival and cell
110 migration [14-19]. Both complexes, mTORC1 and mTORC2, have been linked to
111 the control of protein synthesis, although the role of mTORC2 is not as clearly
112 defined as that of mTORC1 [20,21]. We found that mTORC2 activity, but not
113 mTORC1 activity, is downregulated in the mutant embryo. Similar effects were
114 observed in HEK293T cells which were knocked down for Ric-8B. Altogether these

bioRxiv preprint doi: https://doi.org/10.1101/677054; this version posted June 19, 2019. The copyright holder for this preprint (which was not certified by peer review) is the author/funder, who has granted bioRxiv a license to display the preprint in perpetuity. It is made available under aCC-BY 4.0 International license.

115 results show that Ric-8B is essential for embryogenesis. They also show that
116 depletion of Ric-8B selectively inhibits mTORC2 activity.

117

118 # Results

119 ## Generation of Ric-8B gene trap mice

120 In order to generate mice that are deficient for Ric-8B we obtained two
121 Baygenomics ES cell lines [22], which contain a gene trap vector in the Ric-8B
122 gene. In the RRH188 cell line, the vector is inserted in the intron between exons 3
123 and 4, and in the RRA103 cell line the vector is inserted in the intron between
124 exons 7 and 8 (Fig. 1A). We used these two ES cell lines to produce chimeric
125 mice, but we could only obtain chimeras from the RRH188 cell line. The insertion
126 of the gene trap vector leads to the expression of a chimeric mRNA containing
127 exons 1, 2 and 3 in frame with the β-geo sequence [23]. The resulting Ric-8B
128 fusion protein is likely to be nonfunctional, because it only contains amino acids 1-
129 246 from Ric-8B. Chimeric males were crossed with C57BL/6 females and the
130 agouti-colored offspring were analyzed for transmission of the gene trap vector. As
131 expected, approximately 50% of these mice were heterozygous for the gene trap
132 insertion. These mice develop normally with no signs of deficits, when compared to
133 their wild type siblings.

134

135 ## Ric-8B mutant mice are embryonic lethal

bioRxiv preprint doi: https://doi.org/10.1101/677054; this version posted June 19, 2019. The copyright holder for this preprint (which was not certified by peer review) is the author/funder, who has granted bioRxiv a license to display the preprint in perpetuity. It is made available under aCC-BY 4.0 International license.

Heterozygous mice were intercrossed to generate homozygous mutant mice. Genotyping of the offspring revealed the absence of mice homozygous for the Ric-8B gene mutation (Table 1). In order to determine the time of embryonic death, embryos from heterozygous intercrosses were genotyped at different developmental stages (Fig. 1B, Table 1). We found that homozygous embryos die around embryonic day 10.5.

Table 1. Analysis of offspring and embryos from intercrosses of heterozygous mice. Genotypes were determined by PCR. The number of abnormal or dead embryos is shown in parenthesis.

Stage	Ric-8B$^{wt/wt}$	Ric-8B$^{wt/bgeo}$	Ric-8B$^{bgeo/bgeo}$ (abnormal)	Total #
E7.5	11	22	9	42
E8.5	31	56	22(20)	109
E9.5	100	164	97(82)	361
E10.5	8	40	25(23)	73
E12.5	7	12	1(1)	20
Post natal	29	53	0	82

As mentioned above, two major transcript forms of Ric-8B are expressed in the olfactory epithelium, a full-length Ric-8B isoform and Ric-8BΔ9, an isoform which lacks exon 9 (Fig. 1A) [2]. RT-PCR experiments showed that the Ric-8B gene is expressed in the mouse embryo at early stages of development, and that Ric-8BΔ9 is the predominant isoform present in the embryo, while both isoforms are equally abundant in the olfactory epithelium of adult mice (Fig. 1C, [2]).

bioRxiv preprint doi: https://doi.org/10.1101/677054; this version posted June 19, 2019. The copyright holder for this preprint (which was not certified by peer review) is the author/funder, who has granted bioRxiv a license to display the preprint in perpetuity. It is made available under aCC-BY 4.0 International license.

RT-PCR analysis demonstrated that even though detectable, the levels of Ric-8B mRNA are much lower in the homozygotes (Ric-8B$^{bgeo/bgeo}$) than in the wild type (Ric-8B$^{wt/wt}$) or heterozygous (Ric-8B$^{wt/bgeo}$) embryos (Fig. 1D and E). Accordingly, Western blot analysis of extracts prepared from whole embryos demonstrated that the levels of Ric-8B protein are lower in the homozygous embryos than in wild type or heterozygous embryos (Fig. 1F). The residual levels present in the homozygous embryos is likely to result from the gene knockout technology used [23].

Ric-8B gene expression in the adult mouse

We used the β-geo gene reporter, which is expressed under the control of the Ric-8B promoter, to monitor the Ric-8B gene expression in the heterozygous (Ric-8B$^{wt/bgeo}$) mice. Strong blue staining is detected in the olfactory epithelium, but not in the olfactory bulb, vomeronasal organ or brain (Fig. 2A). Staining can also be detected in the septal organ of Masera, an isolated small patch of sensory epithelium located at the ventral base of the nasal septum [24], which is known to contain olfactory sensory neurons that express Gαolf as well as other canonical olfactory sensory neuron genes [25]. Although no staining was observed in the medial view of the brain (Fig. 2A), when the brain is sectioned in a parasagittal plane, blue staining of the striatum is revealed (Fig. 2B). X-gal staining of sections cut through the nasal cavity shows that β-galactosidase activity is present throughout the olfactory epithelium and in the region where the neurons of the septal organ are located (Fig. 2C, D and F). These results are in agreement with analysis of Ric-8B gene expression by *in situ* hybridization [2], and indicate that the

bioRxiv preprint doi: https://doi.org/10.1101/677054; this version posted June 19, 2019. The copyright holder for this preprint (which was not certified by peer review) is the author/funder, who has granted bioRxiv a license to display the preprint in perpetuity. It is made available under aCC-BY 4.0 International license.

180 expression of the β-geo reporter is indistinguishable from that of the endogenous
181 Ric-8B gene.
182
183 We also examined the Ric-8B gene expression in different tissues of the
184 heterozygous mice. No staining was observed in any of the several analyzed
185 tissues (see S1 Fig). Altogether, these results confirm the previous findings that the
186 expression of the Ric-8B gene is predominantly expressed in a few tissues in the
187 adult mouse. Lower levels of Ric-8B gene expression are however also detectable
188 in several other tissues, as shown in publicly available gene expression data, such
189 as the EMBL-EBI expression Atlas (https://www.ebi.ac.uk/gxa/home) and Mouse
190 ENCODE transcriptome data (https://www.ncbi.nlm.nih.gov/gene/237422/).
191
192 **Ric-8B is required for embryonic growth and development of the cranial**
193 **neural tube**
194 Analysis of the heterozygous embryos showed that expression from the Ric-8B
195 gene promoter is restricted to the cephalic neural folds and neural tube regions
196 (Fig. 3B, E and E'). Notably, the levels of β-galactosidase expression are
197 significantly higher in the Ric-8B$^{bgeo/bgeo}$ embryos when compared to heterozygote
198 embryos (Fig. 3C, F and F'). These results are expected, since the Ric-8B$^{bgeo/bgeo}$
199 embryos carry two copies of the β-geo reporter gene while the Ric-8B$^{wt/bgeo}$
200 embryos have only one copy.
201

bioRxiv preprint doi: https://doi.org/10.1101/677054; this version posted June 19, 2019. The copyright holder for this preprint (which was not certified by peer review) is the author/funder, who has granted bioRxiv a license to display the preprint in perpetuity. It is made available under aCC-BY 4.0 International license.

At E8.5-9.5, heterozygous embryos (Ric-8B$^{wt/bgeo}$, Fig. 3B, E and E') are morphologically similar to that of the wild type embryos (Ric-8B$^{wt/wt}$, Fig. 3A, D and D'). However, from E8.5, great part of homozygous mutant embryos (Ric-8B$^{bgeo/bgeo}$; Fig. 3B, C) are slightly smaller and show phenotypic abnormalities in the prosencephalon. The reduced size of homozygote embryos is emphasized in later stages (Fig. 3J), and the failure in the closure of the cephalic neural tube becomes evident at E9.5 (Fig. 3 F, F'). In order to better visualize the fusion of the cephalic neural folds we performed scanning electron microscopy. Wild type as well as heterozygous E9.5 embryos show normally closed neural tube (Fig. 3G and G', 3H and H'). The Ric-8B$^{bgeo/bgeo}$ embryos, however, do not display fused midline hemispheres (Fig. 3I and I'). These embryos are not able to close the neural tube and usually display open rhombencephalic, mesencephalic and prosencephalic vesicles (Fig. 3I and I'). It is important to note that this 'open brain' phenotype is highly penetrant, shown by ~86% of the analyzed embryos.

Expression of the Ric-8B gene along the embryonic anterior-posterior axis was analyzed in transverse sections of X-gal stained embryos. Staining in Ric-8B$^{wt/bgeo}$ embryos is highly restricted to the notochord, dorsal neural tube in the region of the presumptive brain, and to the ventral region of the neural tube, including the floor plate of the spinal cord (Fig. 4 A-B and E-H). The same regions are strongly stained in Ric-8B$^{bgeo/bgeo}$ embryos, however, less intense staining is also detected all over the neural tube and regions of the adjacent mesoderm (Fig. 4 C and D, I-L). As mentioned above, while the neural tube is normally closed in the Ric-

bioRxiv preprint doi: https://doi.org/10.1101/677054; this version posted June 19, 2019. The copyright holder for this preprint (which was not certified by peer review) is the author/funder, who has granted bioRxiv a license to display the preprint in perpetuity. It is made available under aCC-BY 4.0 International license.

225 8B$^{wt/bgeo}$ embryos, it fails to close in the brain region in Ric-8B$^{bgeo/bgeo}$ embryos
226 (arrows in Fig. 4G and K).

227 Ric-8B expression pattern in the notochord (Fig. 4B) and the floor plate (Fig. 4H,
228 S4A Fig) is highly reminiscent of the sonic hedgehog (*Shh*) expression at the same
229 embryonic stages [26]. However, we found that Shh signaling is not grossly altered
230 in the homozygous Ric-8B mutant embryos (S4B and S4C Figs). *In situ*
231 hybridization on sections of an E10.5 wild type embryo shows that Gαolf is not co-
232 expressed with Ric-8B in the floor plate, while Gαs is highly expressed all over the
233 neural tube (S5A Fig). In addition, quantitative PCR experiments show that
234 expression of Gαolf is not detected in E7.5 - E10.5 in whole embryos (data not
235 shown). These results suggest that Gαs may be the target for Ric-8B in the mouse
236 embryo, instead of Gαolf.
237
238 The expression of the β-geo reporter gene in the neural folds and roof plate at
239 E8.5-E9.5 (Fig. 4) strongly suggest that the deficiency of Ric-8B gene expression is
240 leading to the failure of neural tube closure. Previous studies have shown that this
241 phenotype can result from a variety of embryonic disturbances [27,28], such as
242 abnormalities in the contraction of apical actin microfilaments within neuroepithelial
243 cells [27], or reduced/ increased apoptosis of neuroepithelial cells [27]. We
244 analyzed the distribution of polymerized actin in the neural tubes of wild type and
245 mutant E9.5 embryos, however, no significant differences between wild type and
246 mutant embryos were observed (Fig. 5A). Disturbances in apoptosis were
247 analyzed by immunostaining for activated caspase-3 in E9.5 embryo sections. We

bioRxiv preprint doi: https://doi.org/10.1101/677054; this version posted June 19, 2019. The copyright holder for this preprint (which was not certified by peer review) is the author/funder, who has granted bioRxiv a license to display the preprint in perpetuity. It is made available under aCC-BY 4.0 International license.

found an increased number of apoptotic cells in the neural tube of Ric-8B$^{bgeo/bgeo}$ embryos, as well as in the cranial mesenchyme (Fig. 5B).

We also tested the impact of Ric-8B gene depletion on apoptosis *in vitro*, by using mouse embryonic fibroblasts (MEFs) generated from the Ric-8B mutant embryos. Even though Ric-8B is predominantly expressed in the nervous system (as shown in Figs. 3 and 4), MEFs prepared from wild type embryos also express Ric-8B, although at much lower levels when compared to whole wild type embryos (data not shown). Noticeably, MEF preparations from Ric-8B$^{bgeo/bgeo}$ embryos died within few days in culture. We found that, while the number of dividing cells seems to be unaltered, as revealed by bromodeoxyuridine (BrdU) staining, the number of cells immuno stained for activated caspase-3 is increased in MEFs generated from Ric-8B$^{bgeo/bgeo}$ embryos, when compared to MEFs generated from Ric-8B$^{wt/wt}$ embryos (Fig. 5C). These results indicate that depletion of Ric-8B leads to increased apoptosis.

Cell signaling pathways altered in the Ric-8B mutant embryos

To gain insight into the molecular mechanisms impacted by the mutation in the Ric-8B gene, we sequenced and compared the transcriptomes of mutant and wild type embryos. The 947 differentially expressed genes (FDR < 0.05) (S1 and S2 Tables) were analyzed with Ingenuity Pathway Analysis (IPA) to identify the overrepresented biological pathways among all differentially regulated genes.

bioRxiv preprint doi: https://doi.org/10.1101/677054; this version posted June 19, 2019. The copyright holder for this preprint (which was not certified by peer review) is the author/funder, who has granted bioRxiv a license to display the preprint in perpetuity. It is made available under aCC-BY 4.0 International license.

Unexpectedly, among the top ten canonical pathways that were identified by IPA, the EIF2 signaling, Regulation of eIF4 and p70S6K signaling and mTOR (mechanistic target of rapamycin) signaling pathways were the most significant (Fig. 6A). The mTOR pathway regulates protein synthesis, in addition to a number of other important physiological processes [14,15,29].

In addition, consistent with the role played by Ric-8B in G protein function, different pathways involving GPCRs and G protein signaling such as G Beta Gamma signaling, Gα12/13 signaling, α-Adrenergic signaling and Phospholipase C signaling are also significantly altered in the mutant embryo (S5B Fig).

mTOR signaling in Ric-8B mutant embryos

We next assessed the activity of mTOR in E9.5 embryos by the phosphorylation levels of key downstream targets of both complexes. Akt, a prosurvival kinase, is fully activated through the phosphorylation of Thr308 by phosphoinositide-dependent kinase 1 (PDK1) and of Ser 473 by mTORC2 [30-33]. We found that while phosphorylation of Akt at Thr 308 was not altered in Ric-8B$^{bgeo/bgeo}$ whole embryo lysates, phosphorylation of Akt at Ser 473 catalyzed by mTORC2 was significantly reduced (Fig. 6B-D). The levels of phosphorylation of ribosomal protein S6, a downstream target for mTORC1, were not significantly altered in Ric-8B$^{bgeo/bgeo}$ embryos, suggesting that mTORC1 activity is intact (Fig. 6E). These results indicate that only the activity of mTORC2 is impaired in Ric-8B$^{bgeo/bgeo}$ embryos.

bioRxiv preprint doi: https://doi.org/10.1101/677054; this version posted June 19, 2019. The copyright holder for this preprint (which was not certified by peer review) is the author/funder, who has granted bioRxiv a license to display the preprint in perpetuity. It is made available under aCC-BY 4.0 International license.

Inhibition of mTORC2 function leads to decreased phosphorylation of the FoxO1 and FoxO3a transcription factors, leading to their translocation to the nucleus and subsequent transcription of pro-apoptotic genes [34]. Consistent with this, transcription of the *FoxO3* gene, which is a target for FoxO1/FoxO3 transcription factors [35], is upregulated in the Ric-8B$^{bgeo/bgeo}$ embryos (log fold change = 0.71; FDR= 0.009; S2 Table). As mentioned above, mTORC2 is also involved in the organization of the cytoskeleton, through the regulation of RhoGTPases and PKCα [15]. Notably, signaling pathways involved in actin regulation by Rho GTPases were also identified by the IPA analysis (Fig. 6A). Altogether these results indicate that Ric-8B is required for normal mTORC2 activity during mouse embryogenesis.

mTOR signaling in Ric-8B knockdown cell lines

We next generated conditional shRNA-mediated Ric-8B knockdown HEK293T cell lines and examined mTOR signaling in these cells. shRNAs targeting three different regions of the Ric-8B gene were used (Fig. 7A). Western blot analysis showed that expression of the Ric-8B protein was reduced in all the three generated cell lines when compared to control cells, with the shRNA17 cell line showing the lowest levels (S6 Fig). Knockdown and control cells were starved for 4 hours and then the mTOR signaling pathway was stimulated through addition of 10% FBS for different times before cell lysis. The phosphorylation levels of Akt at Ser 473 and S6 were compared in protein extracts prepared from the Ric-8B shRNA17 cells and control cells. We found that the levels of phosphorylation of Akt

bioRxiv preprint doi: https://doi.org/10.1101/677054; this version posted June 19, 2019. The copyright holder for this preprint (which was not certified by peer review) is the author/funder, who has granted bioRxiv a license to display the preprint in perpetuity. It is made available under aCC-BY 4.0 International license.

314 at Ser 473 are markedly reduced in the knockdown cells (Fig. 7B). As shown for
315 the Ric-8B mutant embryos, no striking differences were observed in the S6
316 phosphorylation levels (Fig. 7B). These results show that not only in the mouse
317 embryo, but also in the HEK293T cells, Ric-8B is required for mTORC2, but not for
318 mTORC1 activity.

319 Finally, because previous work showed that Ric-8B stabilizes expression of Gαs/olf
320 protein subunits in different cell types [7,8,11], we asked whether the Gαs protein
321 is stably expressed in our Ric-8B knockdown cells. Experiments using protein
322 extracts prepared from these cells showed that the levels of the Gαs protein are
323 reduced when compared to the levels found in control cells (Fig. 7C).

324

325

326 ## Discussion

327

328 In this study, we show that the Ric-8B hypomorph embryos fail to close the neural
329 tube at the cephalic region. Our results show that increased apoptosis occurs in
330 the region of the neural tube defect in Ric-8B mutant mice. Expansion of the cranial
331 mesenchyme is required for the elevation of the cranial neural folds, and excessive
332 apoptosis in the mesenchyme would preclude this expansion. Therefore, excessive
333 apoptosis must cause or contribute to the cranial neural tube defect observed in
334 the Ric-8B mutant mice. The finding that MEFs generated from the mutant Ric-8B
335 embryos also show an increased frequency of apoptotic cells, further supports a

bioRxiv preprint doi: https://doi.org/10.1101/677054; this version posted June 19, 2019. The copyright holder for this preprint (which was not certified by peer review) is the author/funder, who has granted bioRxiv a license to display the preprint in perpetuity. It is made available under aCC-BY 4.0 International license.

role for Ric-8B in apoptosis. We found that mTORC2 activity, but not mTORC1 activity, is reduced in the Ric-8B mutant embryos when compared to wild type embryos. Since mTORC2 phosphorylation of Akt at Ser 473 promotes cell survival versus apoptosis [36], decreased activity of mTORC2 could therefore lead to increased apoptosis in the Ric-8B mutant embryo. Further experiments would however be required to determine whether the observed increase in apoptosis is a direct consequence of mTORC2 dysregulation in this case.

Open cephalic tube phenotypes are also seen in embryos that are mutant for a series of different genes, indicating that varied processes are required for successful closure of the neural tube [27,28]. Notably, embryos deficient for the G protein Gβ1 subunit also exhibit similar defects [37], supporting the involvement of G protein mechanisms in these processes. Mutations that lead to the upregulation of the Shh pathway also may result in open cranial tube phenotypes [38]. For example, complete loss of the ciliary Gpr161 leads to increased Shh signaling and lethality by E10.5 with open forebrain and midbrain regions [39]. Loss of Gαs leads to activation of Shh signaling and embryos die at E9.5 with open neural tube and cardiac defects [40]. We found however, that Shh signaling is not severely altered in the Ric-8B homozygous mutants. Still, since these Ric-8B mutants are not null, we cannot exclude the possibility that the residual function of Ric-8B may attenuate the actual Ric-8B null phenotype. Accordingly, knockout of the Ric-8B gene results in embryonic lethality at earlier stages (between E4 and E8.5), indicating that in this case the mice present earlier phenotypes that result in earlier death [7].

bioRxiv preprint doi: https://doi.org/10.1101/677054; this version posted June 19, 2019. The copyright holder for this preprint (which was not certified by peer review) is the author/funder, who has granted bioRxiv a license to display the preprint in perpetuity. It is made available under aCC-BY 4.0 International license.

Several mutant mice have already been generated to study the role played by the mTOR complexes *in vivo*. Interestingly, embryos that are ablated for *Rictor*, a specific component present in mTORC2 that is required for its function, are smaller than their littermates [32,33], a phenotype that is similar to the one shown by Ric-8B mutant embryos (Fig. 4J). Even though *Rictor* null embryos do not show open cranial neural tubes, mice knocked out for *mLST8* fail to develop the cephalic region [32]. mLST8 contains seven WD-40 repeats that are common to Gβ subunits, and is therefore also named GβL (G protein β subunit like protein) [41]. mLST8 is present in both mTORC1 and mTORC2 complexes, but required only for mTORC2 function during development. *Rictor* and *mLST8* deficient embryos are phenotypically similar, they die around E10.5 and show reduced phosphorylation of Akt at Ser473 [32,33]. In addition, in these mutant embryos, phosphorylation of Akt at Thr 308 is not altered when compared to the wild type embryos, as also observed for the Ric-8B mutant embryo [32,33].

The tuberous sclerosis complex (composed of Tsc1 and Tsc2) is a critical negative regulator of mTORC1 and its deficiency promotes constitutive activation of mTORC1, as expected, but also inhibition of mTORC2 [42-44]. This involves a negative feedback catalyzed by mTORC1 downstream targets S6K and GRB10 on IRS-PI3K function upstream to mTORC2 [45,46]. Embryos with mutations in the *Tsc1* and *Tsc2* genes are smaller compared to age-matched controls, and also show exencephaly. These phenotypes are of less magnitude but similar to those seen in the Ric-8B mutant embryos [47-50], suggesting that they may be mediated

bioRxiv preprint doi: https://doi.org/10.1101/677054; this version posted June 19, 2019. The copyright holder for this preprint (which was not certified by peer review) is the author/funder, who has granted bioRxiv a license to display the preprint in perpetuity. It is made available under aCC-BY 4.0 International license.

382 by mTORC2 inhibition rather than constitutive mTORC1 activation. Altogether
383 these findings suggest that Ric-8B mutant embryonic phenotypes may be, at least
384 in part, consequence of impaired mTORC2 signaling.

385 Upstream regulators of mTORC2 are still largely unknown [15,18,29,51]. Our
386 results show that Ric-8B is required for mTORC2 activity, both, in the developing
387 embryo and in HEK293T cells. There is evidence indicating that GPCR signaling
388 can activate the mTOR signaling pathway, but how the signal is relayed within the
389 cell to activate mTORC2 remains unknown. Growth factors activate mTORC2
390 through PI3K-dependent mTORC2-ribosome association, through a mechanism
391 that is still not completely understood [20,21]. GPCR-promoted activation of PI3K is
392 thought to be mediated by Gβγ subunits [52-54]. A study showed that gallein, a
393 pharmacological inhibitor of Gβγ, attenuated CXCR4 chemokine receptor promoted
394 phosphorylation of Akt Ser 473, indicating that Gβγ is required for Akt signaling
395 through this GPCR [55]. A different study showed that Gβγ directly interacts with
396 both, mTORC1 and mTORC2 complexes, raising the possibility that they can
397 activate mTOR independently of PI3K [56].

398 Recent studies have found that adrenergic signaling may induce mTORC2
399 activation [57-59]. One of these studies showed that Akt (Ser473) phosphorylation
400 can be induced in brown adipocytes upon β-adrenergic stimulation in a PI3K-
401 dependent and mTORC1-independent fashion, and via cAMP [57]. These results
402 indicate that GPCR signaling through Gs can activate mTORC2 in some cell types.
403 Even though the precise mechanisms through which Ric-8B is involved in
404 mTORC2 signaling require further investigation, our results suggest that reduced

bioRxiv preprint doi: https://doi.org/10.1101/677054; this version posted June 19, 2019. The copyright holder for this preprint (which was not certified by peer review) is the author/funder, who has granted bioRxiv a license to display the preprint in perpetuity. It is made available under aCC-BY 4.0 International license.

phosphorylation of Akt at Ser473 in the Ric-8B knockdown cells could be due to the lower levels of Gαs expressed in these cells. Noteworthy, however, we found that the Ric-8BΔ9 isoform, which does not interact with Gα subunits but does interact with Gβγ subunits, is the predominant form of Ric-8B expressed in the embryo (Fig. 1C). It is therefore also possible that Gβγ signaling is altered, leading to a defective mTORC2 signaling (Fig. 7D). Finally, our results do not exclude the possibility that Ric-8B and/or Ric-8BΔ9 could have additional targets that are unrelated to G proteins and are yet to be identified.

In summary, our results show that Ric-8B is essential for mouse embryogenesis and is required for the normal development of the nervous system. In addition, they show that deletion of Ric-8B leads to impaired mTORC2 function, and provide evidence for a connection between GPCR/G protein signaling and mTORC2 activity. Extensive studies of the Ric-8B mutants should contribute to unravel the mechanisms that regulate mTORC2 activity, which are still little understood.

Materials and Methods

Animal procedures

bioRxiv preprint doi: https://doi.org/10.1101/677054; this version posted June 19, 2019. The copyright holder for this preprint (which was not certified by peer review) is the author/funder, who has granted bioRxiv a license to display the preprint in perpetuity. It is made available under aCC-BY 4.0 International license.

All procedures undertaken in this study were approved by the University of São Paulo Chemistry Institute's Animal Care and Use Committee, under the protocol #19/2013 and #60/2017.

Gene trap mice

The Baygenomics ES cell lines RRH188 and RRA103 derived from the 129P2Ola/HSD strain were used. The insertion of the gene trap vectors (pGT01xf and pGT11xf, respectively) in the Ric-8B gene was confirmed by RT-PCR, using the vector primer β-geo R together with primer RRH188F in exon 3 or primer RRA103F in exon 7, to detect the corresponding chimeric mRNAs. The cells were injected into C57BL/6 strain blastocysts at the Mutant Mouse Regional Resource Center (MMRRC) at the University of California, Davis (http://www.mmrrc.org) to produce chimeric mice. Chimeric male mice showing high percent chimerism were crossed to C57BL/6 females and the resulting agouti offspring was genotyped by PCR on ear genomic DNA using primers that recognize the gene trap vector (vector F2, and β–geo R). Primer sequences are shown in S3 Fig. The precise site of vector insertion in the third intron of Ric-8B was determined as described in S2 Fig. Heterozygous mice were intercrossed and the resulting mice were genotyped by a multiplex PCR using three primers: the forward primer 188intronF2 in intron 3 and two reverse primers, the VectorR2 primer in the gene trap vector for the Ric-8B KO allele (312 bp PCR product), and the 188intronR2 primer in intron 3 for the WT allele (582 bp PCR product). PCR reactions started with a denaturation step of

bioRxiv preprint doi: https://doi.org/10.1101/677054; this version posted June 19, 2019. The copyright holder for this preprint (which was not certified by peer review) is the author/funder, who has granted bioRxiv a license to display the preprint in perpetuity. It is made available under aCC-BY 4.0 International license.

448 95^{0}C for 3 minutes, followed by 35 cycles of 95^{0}C for 45 s, 68^{0}C for 45 s and 72^{0}C
449 for 1 minute.

450 **X-gal staining of tissues and embryos**

451 X-gal staining was performed as described in [60]. Briefly, for whole mounts,
452 tissues were dissected and incubated on ice for 30 minutes with 100 mM
453 phosphate buffer (pH 7.4), 4% PFA, 2 mM $MgSO_4$, 5 mM EGTA, washed once with
454 100 mM phosphate buffer (pH7.4), 2 mM $MgCl_2$, 5mM EGTA at room temperature
455 and further incubated for 30 minutes with the same buffer. Tissues were then
456 washed twice for 5 minutes at room temperature with 100 mM phosphate buffer
457 (pH 7.4), 2 mM $MgCl_2$, 0.01% sodium deoxycholate, 0.02% NP-40 and incubated
458 for 3 hours (olfactory epithelium), 9 hours (striatum) or overnight (embryos) in the
459 dark at 37^{0}C with 100 mM phosphate buffer (pH 7.4), 2 mM $MgCl_2$, 0.01% sodium
460 deoxycholate, 0.02% NP-40, 5 mM potassium ferricyanide, 5 mM potassium
461 ferrocyanide, 1mg/ml X-gal. For sections, whole mount embryos stained with X-gal
462 were frozen to -20^{0}C in OCT (Sakura TissueTek) and immediately sectioned using
463 a cryostat. It is important to note that we also detected endogenous β-
464 galactosidase activity in the olfactory epithelium of wild type mice, as previously
465 described [61], however, it was observed only after one overnight incubation with
466 X-gal, while staining of the olfactory epithelium from heterozygous RRH188 mice is
467 visible after 3 hours.
468

469 ***In situ* hybridization**

bioRxiv preprint doi: https://doi.org/10.1101/677054; this version posted June 19, 2019. The copyright holder for this preprint (which was not certified by peer review) is the author/funder, who has granted bioRxiv a license to display the preprint in perpetuity. It is made available under aCC-BY 4.0 International license.

Dissected embryos were fixed in 4% PFA for 16 hours at 4°C. Cryopreservation was performed in 30% sucrose, 50% OCT for 2 hours at 4°C. Then, whole mount embryos were frozen in OCT and sectioned using a cryostat. For *in situ* hybridization experiments, sections were fixed in 4% PFA for 10 minutes, washed twice in PBS for 5 minutes and digested with Proteinase K 10 μg/ml for 8 minutes. Then, sections were fixed in 4% PFA for 15 minutes and washed twice in PBS for 5 minutes. The following steps were performed as described in [2].

Western blot

Whole E9.5 embryos or HEK293T cells were lysed with cold RIPA buffer (100 mM Tris pH 7,4; 0,25% sodium deoxycholate; 150 mM NaCl, 1 mM EDTA and 1% NP40 v/v containing 1 X phosphatase inhibitor phoSTOP (Sigma #4906845001) and 1 X protease inhibitor cocktail, Sigma) and 10% SDS-PAGE was used to fractionate proteins. Western blotting was performed by using anti-Gli3 (Proteintech #19949-1-AP), anti-Ric-8B (Atlas #HPA042746), anti-phospho S6 (Cell Signaling #5364), anti S6 (Cell Signaling #2217), anti-phospho-Akt (Ser 473) (Cell Signaling #4060), anti-phospho-Akt (Thr 308) (Cell Signaling#2965), anti-Akt 1 (Millipore #06-885), anti-Akt (pan) (Cell Signaling #2920), anti-Gαs (Santa Cruz #55545), anti-α-tubulin (Sigma #T5168) or anti-β-actin (Santa Cruz #47778) antibodies. Immunoreactivity was detected by incubating the membranes with specific HRP-conjugated secondary antibodies (Cell Signaling), and visualized using a chemiluminescence system (Amersham ECL Prime, GE Healthcare #RPN2133). For the semi-quantitative analysis of phospho-AKT (Ser 473) and

bioRxiv preprint doi: https://doi.org/10.1101/677054; this version posted June 19, 2019. The copyright holder for this preprint (which was not certified by peer review) is the author/funder, who has granted bioRxiv a license to display the preprint in perpetuity. It is made available under aCC-BY 4.0 International license.

493 phosphoS6, the blots were scanned using a gel image capture system to quantify
494 differences via densitometry (Alliance 2.7 system, Alliance 1D capture software,
495 and UVIBand 12.14 analysis software; UVITEC, Cambridge, UK). Values are
496 expressed as percentages of control after normalization with β-actin. Data are
497 expressed as mean ± standard error of the mean (SEM). Statistical analysis was
498 performed by one-way ANOVA followed by Tukey's post hoc test.
499
500 **RT-PCR**
501 RNA was purified from mouse embryos and cDNA synthesis was performed as
502 previously described [2]. The pair of primers Ric-8BFexon3 and Ric-8BRexon5, or
503 RicRTF and RicRTR (see S3 Fig) were used to amplify different regions of the Ric-
504 8B cDNA. The PCR reaction was carried out for 28 cycles, and the PCR products
505 were analyzed in 1% agarose gels.
506
507 **Real-time PCR**
508 Ric-8B gene expression was quantified by real-time PCR using the ABI (USA)
509 7300 Real-Time PCR system, and cDNAs were prepared from E10.5 embryos as
510 previously described [2,62]. Primer sequences were Ric-8BF *forward* 5'-
511 AGCTGGTTCGTCTCATGACAC-3' and Ric-8BR *reverse* 5'-
512 CAGCGTTCCCATAGCCAGTG-3'. All reactions were performed by using a
513 standard real time PCR protocol (1 cycle of 95°C for 10 min, 40 cycles of 95°C for
514 15 s, and 60°C for 1 min). Data was normalized by using β-actin as reference.
515 Relative gene expression between different embryos was then calculated as

bioRxiv preprint doi: https://doi.org/10.1101/677054; this version posted June 19, 2019. The copyright holder for this preprint (which was not certified by peer review) is the author/funder, who has granted bioRxiv a license to display the preprint in perpetuity. It is made available under aCC-BY 4.0 International license.

516 $2^{-\Delta\Delta Ct}$, using the sample of the wild type embryo as calibrator, according to Livak
517 and Schmittgen [63]. Each reaction was performed in triplicate and the standard
518 deviation was inferior to 0.3.
519
520 **Scanning electron microscopy**
521 Embryos were dissected in cold PBS and fixed overnight at 4°C in PBS containing
522 4% paraformaldehyde, 2.5% glutaraldehyde, 1% tannic acid and 5 mM calcium
523 chloride. The embryos were dehydrated through a graded ethanol series and
524 critical point-dried (Balzers CPD 050). After gold-sputtering (20 nm-gold layer)
525 (BalTec CSC 020), the embryos were observed in a Jeol 5310 operating at 15 kV.
526 Digital images were acquired at the resolution of 1024×770 pixels using SEMafore
527 software.
528
529 **Immunostaining**
530 Embryos were fixed overnight at 4°C in 4% PFA, followed by cryoprotection in 30%
531 sucrose, and embedding in OCT (Sakura TissueTek). OCT blocks were sectioned
532 at 14-16 µm using a cryostat. Sections were blocked in 10% FBS, 0.2% Triton-X
533 for 1 hour, followed by incubation with anti-cleaved caspase-3 (Cell Signaling
534 #9661, 1:250) diluted in 1% FBS, 0.2% Triton-X. After incubation, sections were
535 washed with PBS and incubated with Alexa488-conjugated donkey anti-rabbit IgG
536 (Life Technologies #A-21206, 1:300) and Rhodamine Phalloidin diluted in 1% FBS,
537 0.2% Triton-X. Nuclei were stained with DAPI (SIGMA, 0.5 µg/ml).
538
539 **MEFs**

bioRxiv preprint doi: https://doi.org/10.1101/677054; this version posted June 19, 2019. The copyright holder for this preprint (which was not certified by peer review) is the author/funder, who has granted bioRxiv a license to display the preprint in perpetuity. It is made available under aCC-BY 4.0 International license.

MEFs were isolated from E9.5 embryos of each genotype and cultured in DMEM with 10% FBS. Cells were pulsed for 1 hour with 10μM bromodeoxyuridine (Brdu) and fixed in 4% PFA for 20 minutes at room temperature. After fixation, cells were double stained with anti-BrdU (Santa Cruz sc-32323, 1:400) and anti-cleaved caspase-3 primary antibodies (Cell Signaling #9661, 1:250). Nuclei were stained with DAPI (SIGMA, 0.5 μg/ml). Photographs were taken using a Nikon TE300 microscope.

RNA sequencing (RNA-Seq) and signaling pathway analysis

Ribosomal RNA was depleted from total RNA prepared from E10.5 mouse embryos using the RiboMinus Eukaryote Kit for RNA-Seq (Invitrogen). RNA-Seq libraries were prepared using SOLiD Total RNA-Seq Kit, according to the manufacturers' recommendations, and were sequenced on the SOLiD sequencing platform (Life technologies, Carlsbad, CA). Sequences were then aligned to the mouse genome (version GRCm38/mm10) using Tophat [64] with default parameters and gene annotations provided by Ensembl (version 71, [65]). Alignments were filtered with SAMtools [66]. The uniquely mapped reads with minimum mapping quality 20 were used to calculate gene expression, which was generated using Cufflinks [67]. Pathway analysis was performed using Ingenuity Pathway Analysis (IPA, QIAGEN, Redwood City, www.qiagen.com/ingenuity). The overrepresented pathways, shown in Fig. 6A, met the IPA cut-off threshold for significance (p-value < 0.05). Analysis was run by using all default settings for the selection of dataset, no fold-change cut-off, FDR <0.05 and P-value < 0.05.

bioRxiv preprint doi: https://doi.org/10.1101/677054; this version posted June 19, 2019. The copyright holder for this preprint (which was not certified by peer review) is the author/funder, who has granted bioRxiv a license to display the preprint in perpetuity. It is made available under aCC-BY 4.0 International license.

563

564 **Knock down experiments**

565 To knockdown Ric-8B expression in HEK293T cells we used the SMARTvector
566 Inducible Human RIC8B shRNA (V3SH11252-227737126
567 GGATGTTTCGATGGGCTCG; V3SH11252-229071976
568 TAAACAATGACGAAGGACA; V3SH11252-229376731
569 CTGAGTACCAATTATCTCC (Dharmacon). For the experiments shown in Figure
570 9B cells were plated in Dulbecco's Modified Eagle's Medium (DMEM)
571 supplemented with 10% of fetal bovine serum (FBS) and doxycycline 1,0 µg/mL.
572 Three days later, medium was removed and cells were washed twice with PBS 1x.
573 Cells were starved in DMEM without FBS for 4 hours and then stimulated with
574 DMEM 10% FBS for different times.

575

576 ## Acknowledgements

577 We are very grateful to Chao Yun Irene Yan, Deborah Schechtman and Hiroaki
578 Matsunami for helpful comments and suggestions. We also thank Silvania Neves
579 and Renata Spaluto for assistance with animal care and Erica Bandeira for
580 technical assistance. This work was supported by grants from Fundação de
581 Amparo à Pesquisa do Estado de São Paulo (FAPESP#16/24471-0; #
582 2014/15495-8), CNPq and CAPES.

583

584 ## References

bioRxiv preprint doi: https://doi.org/10.1101/677054; this version posted June 19, 2019. The copyright holder for this preprint (which was not certified by peer review) is the author/funder, who has granted bioRxiv a license to display the preprint in perpetuity. It is made available under aCC-BY 4.0 International license.

585 1. Tall GG, Krumins AM, Gilman AG (2003) Mammalian Ric-8A (synembryn) is a
586 heterotrimeric Ga protein guanine nucleotide exchange factor. J Biol Chem
587 278: 8356-8362.
588 2. Von Dannecker L, Mercadante A, Malnic B (2005) Ric-8B, an olfactory putative
589 GTP exchange factor, amplifies signal transduction through the olfactory-
590 specific G-protein Gaolf. J Neurosci 25: 3793-3800.
591 3. Chan P, Gabay M, Wright FA, Tall GG (2011) Ric-8B is a GTP-dependent G
592 protein alphas guanine nucleotide exchange factor. J Biol Chem 286:
593 19932-19942.
594 4. Jones DT, Reed RR (1989) Golf: an olfactory neuron-specific G-protein involved
595 in odorant signal transduction. Science 244: 790-795.
596 5. Belluscio L, Gold GH, Nemes A, Axel R (1998) Mice deficient in G(olf) are
597 anosmic. Neuron 20: 69-81.
598 6. Zhuang X, Belluscio L, Hen R (2000) Golfa mediates dopamine D1 receptor
599 signaling. J Neurosci 20: RC91.
600 7. Gabay M, Pinter ME, Wright FA, Chan P, Murphy AJ, et al. (2011) Ric-8 proteins
601 are molecular chaperones that direct nascent G protein alpha subunit
602 membrane association. Sci Signal 4: ra79.
603 8. Nagai Y, Nishimura A, Tago K, Mizuno N, Itoh H (2010) Ric-8B stabilizes the
604 alpha subunit of stimulatory G protein by inhibiting its ubiquitination. J Biol
605 Chem 285: 11114-11120.
606 9. Zhuang H, Matsunami H (2007) Synergism of accessory factors in functional
607 expression of mammalian odorant receptors. J Biol Chem 282: 15284-
608 15293.
609 10. Kerr D, Von Dannecker L, Davalos M, Michaloski J, Malnic B (2008) Ric-8B
610 interacts with Gaolf and Gg13 and co-localizes with Gaolf, Gb1 and Gg13 in
611 the cilia of olfactory sensory neurons. Mol Cell Neurosci 38: 341-348.
612 11. Von Dannecker L, Mercadante A, Malnic B (2006) Ric-8B promotes functional
613 expression of odorant receptors. Proc Natl Acad Sci USA 103: 9310-9314.
614 12. Masuho I, Ostrovskaya O, Kramer GM, Jones CD, Xie K, et al. (2015) Distinct
615 profiles of functional discrimination among G proteins determine the actions
616 of G protein-coupled receptors. Sci Signal 8: ra123.
617 13. Machado CF, Nagai MH, Lyra CS, Reis-Silva TM, Xavier AM, et al. (2017)
618 Conditional Deletion of Ric-8b in Olfactory Sensory Neurons Leads to
619 Olfactory Impairment. J Neurosci 37: 12202-12213.
620 14. Hung CM, Garcia-Haro L, Sparks CA, Guertin DA (2012) mTOR-dependent cell
621 survival mechanisms. Cold Spring Harb Perspect Biol 4.
622 15. Laplante M, Sabatini DM (2012) mTOR signaling in growth control and disease.
623 Cell 149: 274-293.
624 16. Sarbassov DD, Ali SM, Kim DH, Guertin DA, Latek RR, et al. (2004) Rictor, a
625 novel binding partner of mTOR, defines a rapamycin-insensitive and raptor-
626 independent pathway that regulates the cytoskeleton. Curr Biol 14: 1296-
627 1302.
628 17. Jacinto E, Loewith R, Schmidt A, Lin S, Ruegg MA, et al. (2004) Mammalian
629 TOR complex 2 controls the actin cytoskeleton and is rapamycin insensitive.
630 Nat Cell Biol 6: 1122-1128.

bioRxiv preprint doi: https://doi.org/10.1101/677054; this version posted June 19, 2019. The copyright holder for this preprint (which was not certified by peer review) is the author/funder, who has granted bioRxiv a license to display the preprint in perpetuity. It is made available under aCC-BY 4.0 International license.

18. Cybulski N, Hall MN (2009) TOR complex 2: a signaling pathway of its own. Trends Biochem Sci 34: 620-627.
19. Xie J, Wang X, Proud CG (2018) Who does TORC2 talk to? Biochem J 475: 1721-1738.
20. Oh WJ, Wu CC, Kim SJ, Facchinetti V, Julien LA, et al. (2010) mTORC2 can associate with ribosomes to promote cotranslational phosphorylation and stability of nascent Akt polypeptide. EMBO J 29: 3939-3951.
21. Zinzalla V, Stracka D, Oppliger W, Hall MN (2011) Activation of mTORC2 by association with the ribosome. Cell 144: 757-768.
22. Stryke D, Kawamoto M, Huang CC, Johns SJ, King LA, et al. (2003) BayGenomics: a resource of insertional mutations in mouse embryonic stem cells. Nucleic Acids Res 31: 278-281.
23. Stanford WL, Cohn JB, Cordes SP (2001) Gene-trap mutagenesis: past, present and beyond. Nat Rev Genet 2: 756-768.
24. Munger SD, Leinders-Zufall T, Zufall F (2009) Subsystem organization of the mammalian sense of smell. Annu Rev Physiol 71: 115-140.
25. Ma M, Grosmaitre X, Iwema CL, Baker H, Greer CA, et al. (2003) Olfactory signal transduction in the mouse septal organ. J Neurosci 23: 317-324.
26. Roelink H, Porter JA, Chiang C, Tanabe Y, Chang DT, et al. (1995) Floor plate and motor neuron induction by different concentrations of the amino-terminal cleavage product of sonic hedgehog autoproteolysis. Cell 81: 445-455.
27. Copp AJ (2005) Neurulation in the cranial region--normal and abnormal. J Anat 207: 623-635.
28. Copp AJ, Greene ND, Murdoch JN (2003) The genetic basis of mammalian neurulation. Nat Rev Genet 4: 784-793.
29. Saxton RA, Sabatini DM (2017) mTOR Signaling in Growth, Metabolism, and Disease. Cell 168: 960-976.
30. Hresko RC, Mueckler M (2005) mTOR.RICTOR is the Ser473 kinase for Akt/protein kinase B in 3T3-L1 adipocytes. J Biol Chem 280: 40406-40416.
31. Sarbassov DD, Guertin DA, Ali SM, Sabatini DM (2005) Phosphorylation and regulation of Akt/PKB by the rictor-mTOR complex. Science 307: 1098-1101.
32. Guertin DA, Stevens DM, Thoreen CC, Burds AA, Kalaany NY, et al. (2006) Ablation in mice of the mTORC components raptor, rictor, or mLST8 reveals that mTORC2 is required for signaling to Akt-FOXO and PKCalpha, but not S6K1. Dev Cell 11: 859-871.
33. Shiota C, Woo JT, Lindner J, Shelton KD, Magnuson MA (2006) Multiallelic disruption of the rictor gene in mice reveals that mTOR complex 2 is essential for fetal growth and viability. Dev Cell 11: 583-589.
34. Calnan DR, Brunet A (2008) The FoxO code. Oncogene 27: 2276-2288.
35. van der Vos KE, Coffer PJ (2011) The extending network of FOXO transcriptional target genes. Antioxid Redox Signal 14: 579-592.
36. Jacinto E, Facchinetti V, Liu D, Soto N, Wei S, et al. (2006) SIN1/MIP1 maintains rictor-mTOR complex integrity and regulates Akt phosphorylation and substrate specificity. Cell 127: 125-137.

bioRxiv preprint doi: https://doi.org/10.1101/677054; this version posted June 19, 2019. The copyright holder for this preprint (which was not certified by peer review) is the author/funder, who has granted bioRxiv a license to display the preprint in perpetuity. It is made available under aCC-BY 4.0 International license.

677 37. Okae H, Iwakura Y (2010) Neural tube defects and impaired neural progenitor
678 cell proliferation in Gbeta1-deficient mice. Dev Dyn 239: 1089-1101.
679 38. Murdoch JN, Copp AJ (2010) The relationship between sonic Hedgehog
680 signaling, cilia, and neural tube defects. Birth Defects Res A Clin Mol Teratol
681 88: 633-652.
682 39. Mukhopadhyay S, Wen X, Ratti N, Loktev A, Rangell L, et al. (2013) The ciliary
683 G-protein-coupled receptor Gpr161 negatively regulates the Sonic
684 hedgehog pathway via cAMP signaling. Cell 152: 210-223.
685 40. Regard JB, Malhotra D, Gvozdenovic-Jeremic J, Josey M, Chen M, et al.
686 (2013) Activation of Hedgehog signaling by loss of GNAS causes
687 heterotopic ossification. Nat Med 19: 1505-1512.
688 41. Rodgers BD, Levine MA, Bernier M, Montrose-Rafizadeh C (2001) Insulin
689 regulation of a novel WD-40 repeat protein in adipocytes. J Endocrinol 168:
690 325-332.
691 42. Huang J, Dibble CC, Matsuzaki M, Manning BD (2008) The TSC1-TSC2
692 complex is required for proper activation of mTOR complex 2. Mol Cell Biol
693 28: 4104-4115.
694 43. Huang J, Wu S, Wu CL, Manning BD (2009) Signaling events downstream of
695 mammalian target of rapamycin complex 2 are attenuated in cells and
696 tumors deficient for the tuberous sclerosis complex tumor suppressors.
697 Cancer Res 69: 6107-6114.
698 44. Carson RP, Van Nielen DL, Winzenburger PA, Ess KC (2012) Neuronal and
699 glia abnormalities in Tsc1-deficient forebrain and partial rescue by
700 rapamycin. Neurobiol Dis 45: 369-380.
701 45. Hsu PP, Kang SA, Rameseder J, Zhang Y, Ottina KA, et al. (2011) The mTOR-
702 regulated phosphoproteome reveals a mechanism of mTORC1-mediated
703 inhibition of growth factor signaling. Science 332: 1317-1322.
704 46. Yu Y, Yoon SO, Poulogiannis G, Yang Q, Ma XM, et al. (2011)
705 Phosphoproteomic analysis identifies Grb10 as an mTORC1 substrate that
706 negatively regulates insulin signaling. Science 332: 1322-1326.
707 47. Kobayashi T, Minowa O, Sugitani Y, Takai S, Mitani H, et al. (2001) A germ-
708 line Tsc1 mutation causes tumor development and embryonic lethality that
709 are similar, but not identical to, those caused by Tsc2 mutation in mice. Proc
710 Natl Acad Sci U S A 98: 8762-8767.
711 48. Wilson C, Idziaszczyk S, Parry L, Guy C, Griffiths DF, et al. (2005) A mouse
712 model of tuberous sclerosis 1 showing background specific early post-natal
713 mortality and metastatic renal cell carcinoma. Hum Mol Genet 14: 1839-
714 1850.
715 49. Kobayashi T, Minowa O, Kuno J, Mitani H, Hino O, et al. (1999) Renal
716 carcinogenesis, hepatic hemangiomatosis, and embryonic lethality caused
717 by a germ-line Tsc2 mutation in mice. Cancer Res 59: 1206-1211.
718 50. Onda H, Lueck A, Marks PW, Warren HB, Kwiatkowski DJ (1999) Tsc2(+/-)
719 mice develop tumors in multiple sites that express gelsolin and are
720 influenced by genetic background. J Clin Invest 104: 687-695.
721 51. Shimobayashi M, Hall MN (2014) Making new contacts: the mTOR network in
722 metabolism and signalling crosstalk. Nat Rev Mol Cell Biol 15: 155-162.

bioRxiv preprint doi: https://doi.org/10.1101/677054; this version posted June 19, 2019. The copyright holder for this preprint (which was not certified by peer review) is the author/funder, who has granted bioRxiv a license to display the preprint in perpetuity. It is made available under aCC-BY 4.0 International license.

52. Dbouk HA, Vadas O, Shymanets A, Burke JE, Salamon RS, et al. (2012) G protein-coupled receptor-mediated activation of p110beta by Gbetagamma is required for cellular transformation and invasiveness. Sci Signal 5: ra89.
53. Leopoldt D, Hanck T, Exner T, Maier U, Wetzker R, et al. (1998) Gbetagamma stimulates phosphoinositide 3-kinase-gamma by direct interaction with two domains of the catalytic p110 subunit. J Biol Chem 273: 7024-7029.
54. O'Hayre M, Degese MS, Gutkind JS (2014) Novel insights into G protein and G protein-coupled receptor signaling in cancer. Curr Opin Cell Biol 27: 126-135.
55. Verma R, Marchese A (2015) The endosomal sorting complex required for transport pathway mediates chemokine receptor CXCR4-promoted lysosomal degradation of the mammalian target of rapamycin antagonist DEPTOR. J Biol Chem 290: 6810-6824.
56. Robles-Molina E, Dionisio-Vicuna M, Guzman-Hernandez ML, Reyes-Cruz G, Vazquez-Prado J (2014) Gbetagamma interacts with mTOR and promotes its activation. Biochem Biophys Res Commun 444: 218-223.
57. Albert V, Svensson K, Shimobayashi M, Colombi M, Munoz S, et al. (2016) mTORC2 sustains thermogenesis via Akt-induced glucose uptake and glycolysis in brown adipose tissue. EMBO Mol Med 8: 232-246.
58. Mukaida S, Evans BA, Bengtsson T, Hutchinson DS, Sato M (2017) Adrenoceptors promote glucose uptake into adipocytes and muscle by an insulin-independent signaling pathway involving mechanistic target of rapamycin complex 2. Pharmacol Res 116: 87-92.
59. Sato M, Evans BA, Sandstrom AL, Chia LY, Mukaida S, et al. (2018) alpha1A-Adrenoceptors activate mTOR signalling and glucose uptake in cardiomyocytes. Biochem Pharmacol 148: 27-40.
60. Mombaerts P, Wang F, Dulac C, Chao S, Nemes A, et al. (1996) Visualizing an olfactory sensory map. Cell 87: 675-686.
61. Liberles S, Buck L (2006) A second class of chemosensory receptors in the olfactory epithelium. Nature 442: 645-650.
62. Michaloski J, Galante P, Malnic B (2006) Identification of potential regulatory motifs in odorant receptor genes by analysis of promoter sequences. Genome Research 16: 1091-1098.
63. Livak KJ, Schmittgen TD (2001) Analysis of relative gene expression data using real-time quantitative PCR and the 2(-Delta Delta C(T)) Method. Methods 25: 402-408.
64. Trapnell C, Pachter L, Salzberg SL (2009) TopHat: discovering splice junctions with RNA-Seq. Bioinformatics 25: 1105-1111.
65. Yates A, Akanni W, Amode MR, Barrell D, Billis K, et al. (2016) Ensembl 2016. Nucleic Acids Res 44: D710-716.
66. Li H, Handsaker B, Wysoker A, Fennell T, Ruan J, et al. (2009) The Sequence Alignment/Map format and SAMtools. Bioinformatics 25: 2078-2079.
67. Trapnell C, Roberts A, Goff L, Pertea G, Kim D, et al. (2012) Differential gene and transcript expression analysis of RNA-seq experiments with TopHat and Cufflinks. Nat Protoc 7: 562-578.

bioRxiv preprint doi: https://doi.org/10.1101/677054; this version posted June 19, 2019. The copyright holder for this preprint (which was not certified by peer review) is the author/funder, who has granted bioRxiv a license to display the preprint in perpetuity. It is made available under aCC-BY 4.0 International license.

768 68. Wang B, Fallon JF, Beachy PA (2000) Hedgehog-regulated processing of Gli3
769 produces an anterior/posterior repressor gradient in the developing
770 vertebrate limb. Cell 100: 423-434.
771

772

bioRxiv preprint doi: https://doi.org/10.1101/677054; this version posted June 19, 2019. The copyright holder for this preprint (which was not certified by peer review) is the author/funder, who has granted bioRxiv a license to display the preprint in perpetuity. It is made available under aCC-BY 4.0 International license.

773 # Figure Legends

774

775 **Fig 1. Ric-8B gene trap mice.** (A) The genomic structure of the Ric-8B gene is
776 shown, with its ten exons (1-10) and nine introns (between the exons) and the
777 insertion sites of the gene trap vector in the ES cell lines RRH188 and RRA103.
778 The insertion of the gene trap vector in intron 3 in the RRH188 cell line leads to the
779 expression of chimeric mRNA containing exons 1, 2 and 3 in frame with the β-geo
780 sequence. The locations of the primers used for PCR-based genotyping are
781 indicated. SA: splice acceptor site. The Ric-8BΔ9 isoform lacks exon 9 (indicated in
782 grey), is indicated. B) Multiplex PCR-based genotyping of the embryos obtained
783 from intercrossing of heterozygous mice using one forward primer (188intronF2)
784 and two reverse primers (VectorR2 and 188intronR2). A 312 bp PCR product is
785 expected for the mutant allele, and a 582 bp PCR product is expected for the wild
786 type allele. Representative analyzed embryos showed the following genotypes:
787 Ric-8B$^{wt/wt}$ (wild type, lanes 1, 3 and 5), Ric-8B$^{wt/bgeo}$ (heterozygote, lanes 2 and 4)
788 and Ric-8B$^{bgeo/bgeo}$ (homozygous, lanes 6 and 7). (C) Ric-8B gene expression in
789 the mouse embryo. RT-PCR was conducted to amplify Ric-8B and Ric-8BΔ9
790 transcripts from RNA prepared from wild type mouse embryos at different
791 developmental stages. The PCR product sizes expected using the pair of primers
792 that flank the ninth exon (A) are 462 bp (Ric-8B) and 342 bp (Ric-8BΔ9). (D) RT-
793 PCR was conducted to amplify the regions between exon 3 and exon 5 (1) and
794 exon 7 and exon 10 (2) of Ric-8B and actin (3) from embryos with different
795 genotypes as indicated. (E) Real-time PCR was conducted to compare the

bioRxiv preprint doi: https://doi.org/10.1101/677054; this version posted June 19, 2019. The copyright holder for this preprint (which was not certified by peer review) is the author/funder, who has granted bioRxiv a license to display the preprint in perpetuity. It is made available under aCC-BY 4.0 International license.

796 expression levels of the Ric-8B gene in wild type (Ric-8B$^{wt/wt}$), heterozygotes (Ric-
797 8B$^{wt/bgeo}$) and homozygous (Ric-8B$^{bgeo/bgeo}$) mutant embryos. Transcript levels were
798 normalized to β-actin levels and are shown relative to the expression levels in wild
799 type embryos. (F) Western blot analysis of protein extracts from embryos with the
800 different genotypes using anti-Ric-8B antibodies. α-tubulin was used as a loading
801 control.

802

803 **Fig 2. Ric-8B expression in the adult Ric-8B$^{wt/bgeo}$ mouse as revealed by X-gal**
804 **staining.** (A) Sagittal whole-mount view of the nasal cavity and brain stained with
805 X-gal. Blue staining can be detected in the olfactory epithelium (OE) and septal
806 organ (SO), but not in the olfactory bulb (OB) nor in the vomeronasal organ (VNO).
807 (B) The brain region is cut in a parasagittal plane, revealing blue staining of the
808 striatum. (C-G) X-gal staining of sections cut through the nasal cavity of Ric-8B
809 $^{wt/bgeo}$ mice (C, D and F) or Ric-8B $^{wt/wt}$ mice (E and G). X-gal staining is present
810 throughout the olfactory epithelium (C, D and F), and in the septal organ region
811 (arrow in D). In the same experimental conditions, no staining is observed in the
812 wild type tissues. Sections in A-G were taken from the regions indicated in the
813 schematic representation of the mouse brain.

814

815 **Fig 3. Ric-8B mutant embryos are smaller and show defective neural tube**
816 **closure in the cephalic region.** (A-F´) Wild type (Ric-8B$^{wt/wt}$), heterozygous (Ric-
817 8B$^{wt/bgeo}$) or homozygous (Ric-8B$^{bgeo/bgeo}$) embryos at E8.5 or E9.5 stained with X-
818 gal are shown (not shown in scale). Ventral (D-F) and dorsal (D'-F') views of the

bioRxiv preprint doi: https://doi.org/10.1101/677054; this version posted June 19, 2019. The copyright holder for this preprint (which was not certified by peer review) is the author/funder, who has granted bioRxiv a license to display the preprint in perpetuity. It is made available under aCC-BY 4.0 International license.

819 embryos are shown. In the Ric-8B$^{bgeo/bgeo}$ embryos, the cephalic neural folds are
820 not fused (white arrows) but the other regions of the neural tube are normally
821 closed (F, F'). (G-I) Wild type (Ric-8B$^{wt/wt}$), heterozygous (Ric-8B$^{wt/bgeo}$) or
822 homozygous (Ric-8B$^{bgeo/bgeo}$) embryos were examined by scanning electron
823 microscopy at E9.5. G', H' and I' are magnified regions from G, H and I,
824 respectively. P (prosencephalon), BA (first branchial arch). Scale bars in G- I
825 represent 100 μm, in G'-I', 50 μm. (J) Representative images of a wild type and a
826 homozygous mutant embryo (shown in scale).

827

828 **Fig 4. Ric-8B expression in the embryo is predominant in the nervous system**
829 **.** Upper panels: sagittal views of a Ric-8B$^{wt/bgeo}$ embryo (A) or a Ric-8B $^{bgeo/bgeo}$
830 embryo (C) at E8.5. The lines indicate the levels at which the sections were cut
831 (shown in B and D). In the Ric-8B$^{wt/bgeo}$ embryo (A and B), blue staining is detected
832 in the neural folds in the brain region (asterisk) and in the notochord (nc). In the
833 Ric-8B$^{bgeo/bgeo}$ embryo (C and D) blue staining is detected in the same regions as in
834 the Ric-8B$^{wt/bgeo}$ embryo, however the staining is stronger and expanded.
835 Lower panels: sagittal and ventral views of a Ric-8B$^{wt/bgeo}$ embryo (E and F) or a
836 Ric-8B$^{bgeo/bgeo}$ embryo (I and J) at E9.5. In the Ric-8B$^{wt/bgeo}$ embryo (E-H), blue
837 staining is detected in the neural fold fusion in the brain region (arrows) and in the
838 floor plate region (fp). Note that the neural tube is closed (arrow in G). (H) Higher
839 magnification of the neural tube in the Ric-8B$^{wt/bgeo}$ embryo showing strong blue
840 staining in the floor plate region and weaker staining in the notochord. In the Ric-
841 8B$^{bgeo/bgeo}$ embryo (I- L) blue staining is detected in the same regions as in the Ric-

bioRxiv preprint doi: https://doi.org/10.1101/677054; this version posted June 19, 2019. The copyright holder for this preprint (which was not certified by peer review) is the author/funder, who has granted bioRxiv a license to display the preprint in perpetuity. It is made available under aCC-BY 4.0 International license.

842 8B$^{wt/bgeo}$ embryo; however, the staining is stronger and expanded. Note that the
843 neural tube is not closed in the anterior region of the head (arrows in K) but are
844 normally closed at the more caudal regions. (L) Higher magnification of the neural
845 tube in the Ric-8B$^{bgeo/bgeo}$ embryo showing strong blue staining in both the floor
846 plate (fp) and notochord (nc) regions. Me (mesenchyme).
847
848 **Fig 5. Increased apoptosis in Ric-8B$^{bgeo/bgeo}$ embryos and MEFs.** (A)
849 Transverse sections of E9.5 embryos stained with rhodamine-conjugated phalloidin
850 (red) show that actin filament (F-actin) is highly concentrated in the apical region of
851 the neural tube in wild type, heterozygous and mutant embryos. (B) Transverse
852 sections of E9.5 embryos stained for active caspase 3 (green). Ric-8B$^{bgeo/bgeo}$
853 embryos show an increased number of apoptotic cells in the mesenchyme and
854 neuroepithelium when compared to wild type or heterozygous embryos. DAPI was
855 used to stain the nuclei. Forebrain (fb); mesenchyme (me); midbrain (mb);
856 hindbrain (hb); neuroepithelium (ne). The approximate localizations of the sections
857 are indicated to the right. (C) MEFs were generated from Ric-8B$^{wt/wt}$ (n=2) or Ric-
858 8B$^{bgeo/bgeo}$ (n=1) embryos were double stained for BrdU (red) and activated
859 caspase-3 (green). The percentages of cells labeled in each case are indicated in
860 the graph.
861
862 **Fig 6. Phosphorylation of Akt (Ser 473) is decreased in Ric-8B$^{bgeo/bgeo}$**
863 **embryos.** (A) Cell signaling pathways predicted to be altered in the Ric-8B mutant
864 embryos. Top 10 altered signaling pathways, as predicted by IPA, are shown. The
865 ranking was based on the p values derived from the Fisher's exact test (IPA). The

bioRxiv preprint doi: https://doi.org/10.1101/677054; this version posted June 19, 2019. The copyright holder for this preprint (which was not certified by peer review) is the author/funder, who has granted bioRxiv a license to display the preprint in perpetuity. It is made available under aCC-BY 4.0 International license.

x axis displays the – (log) p value. (B) Western blot of P-Akt Ser 473 and total Akt1 content in E9.5 embryos from the different Ric-8B genotypes. β-actin was used as loading control. (C) Western blot analysis of P-Akt Thr308 in E9.5 embryos compared to pan-Akt. (D) Semi-quantitative analysis of Akt (Ser 473) phosphorylation in E9.5 embryos. The graph shows the quantification of the ratio of P-Akt Ser 473 compared to pan-Akt. Values are expressed relative to wild type embryo levels and shown as mean +/- S.E.M. (each dot represents an embryo), *, $P<0.05$. A representative Western blot is shown below the graph. (E) Semi-quantitative analysis of S6 phosphorylation in E9.5 embryos. The graph shows the quantification of the ratio of P-S6 compared to total S6. Values are expressed relative to wild type embryo levels and shown as mean +/- S.E.M. (each dot represents an embryo). A representative Western blot is shown below the graph.

Fig 7. Ric-8B is required for mTORC2 activation in HEK293T cells. (A) Schematic representation of the Ric-8B gene structure showing the regions targeted by the shRNAs used to knockdown endogenous expression of Ric-8B in HEK293T cells. (B) HEK293T cell lines containing a control shRNA (shRNA for luciferase) or the Ric-8B shRNA17 were starved for 4 hours and stimulated with FBS for 5, 15, 30 or 45 minutes. Total protein lysates were analyzed in Western blot experiments for the expression of the indicated proteins. (C) Total lysates prepared from HEK293T cell lines expressing a control shRNA, Ric-8B shRNA16 or Ric-8B shRNA17 were analyzed in Western blot experiments for the expression of Gαs. (D) Schematic representation of how Ric-8B may act to regulate mTORC2

bioRxiv preprint doi: https://doi.org/10.1101/677054; this version posted June 19, 2019. The copyright holder for this preprint (which was not certified by peer review) is the author/funder, who has granted bioRxiv a license to display the preprint in perpetuity. It is made available under aCC-BY 4.0 International license.

889 activity. Growth factors activate PI3K at the cell membrane leading to the
890 production of PIP3, recruitment of Akt and PDK1 and phosphorylation of Akt at
891 Threonine 308 by PDK1. As more recently shown, mTORC2 can be activated via
892 GPCR signaling. Depletion of Ric-8B impairs function and/or stability of Gα and
893 Gβγ subunits. As a consequence, phosphorylation of Akt at Serine 473 by
894 mTORC2 is reduced. The exact mechanism through which G protein is required for
895 mTORC2 activity remains to be elucidated (dashed arrow). Akt-Ser 473
896 phosphorylation is known to be required for mTORC2 function in cell survival [36].
897 Ric-8B may also have targets that are unrelated to G proteins and are yet to be
898 identified. Phosphorylated substrates analyzed in our experiments are indicated in
899 green.
900
901

902 ## Supporting Information

903 **S1 Fig. Expression of Ric-8B as revealed by β-galactosidase activity in**
904 **different mouse tissues.** The table shows the results obtained by whole-mount X-
905 gal staining of adult Ric-8B$^{wt/bgeo}$ mouse tissues. (+) blue staining; (-) no staining
906 was detected. Some of the analyzed tissues (prostate, intestine, kidney, testis and
907 seminal vesicle) showed endogenous β-galactosidase activity.
908

909 **S2 Fig. Identification of the precise site of vector insertion in the Ric-8B**
910 **gene.** The locations of the primers used for the identification of the site of insertion
911 of the gene trap vector are indicated. Different pairs of primers were used in PCR

bioRxiv preprint doi: https://doi.org/10.1101/677054; this version posted June 19, 2019. The copyright holder for this preprint (which was not certified by peer review) is the author/funder, who has granted bioRxiv a license to display the preprint in perpetuity. It is made available under aCC-BY 4.0 International license.

912 reactions with genomic DNA prepared from heterozygous mice as indicated. PCR
913 products were only obtained for the 188intronF1/Vector R and 188intronF2/ Vector
914 R pairs of primers, indicating that the vector is inserted ~150 bp downstream to the
915 region matched by the primer 188intronF2.

916 **S3 Fig.- Primer sequences.** List of primer sequences used for genotyping of the
917 embryos and RT-PCR experiments.

918 **S4 Fig. Shh signaling in Ric-8B $^{bgeo/bgeo}$ embryos.** (A) Transverse sections cut
919 through the neural tubes of X-gal stained Ric-8B$^{wt/bgeo}$ embryos at different
920 developmental stages shows that β-galactosidase activity is restricted to the floor
921 plate**.** (B) The expression of the floor plate markers Shh and FoxA2, in addition to
922 Ptch1, a direct target of the Shh signaling pathway, was indistinguishable between
923 the neural tubes from E9.5 Ric-8B$^{wt/wt}$ and Ric-8B$^{bgeo/bgeo}$ embryos, indicating that
924 the most ventral neural types are normally specified in Ric-8B$^{bgeo/bgeo}$ embryos.
925 Transverse section cut through the neural tubes were hybridized with antisense
926 probes specific for Shh, FoxA2 and Ptch1. (C) The Gli3 protein is one of the major
927 transcription factors that mediate the transcriptional effects of Shh signaling. In the
928 absence of Shh signaling, Gli3 is proteolytically processed to produce a form that
929 acts as a transcriptional repressor [68]. Western blotting with antibody against Gli3
930 was used to analyze total protein extracts prepared from E9.5 whole embryos. The
931 amounts of both the activator (Gli3 FL, 230 kDa) and repressor (Gli3 R, 83 kDa)
932 forms of Gli3 in Ric-8B$^{bgeo/bgeo}$ embryos are not different from the ones shown by
933 wild type or heterozygous embryos. Quantification of relative amounts of Gli3 FL

bioRxiv preprint doi: https://doi.org/10.1101/677054; this version posted June 19, 2019. The copyright holder for this preprint (which was not certified by peer review) is the author/funder, who has granted bioRxiv a license to display the preprint in perpetuity. It is made available under aCC-BY 4.0 International license.

and Gli3 R normalized to respective α-tubulin levels is shown at the bottom of the blot. Gli3 FL (Gli3 full length); Gli3 R (Gli3 repressor).

S5 Fig. Signaling pathways involving G proteins altered in the Ric-8B mutant embryos. (A) Gα subunits and Ric-8B gene expression in the embryo. Sections cut through the neural tube of an E10.5 wild type embryo were hybridized with digoxigenin-labeled antisense RNA probes for Ric-8B, Gαolf and Gαs, as indicated. (B) Signaling pathways involving G proteins that are altered in the Ric-8B mutant embryos, as identified by IPA, are shown.

S6 Fig. Ric-8B protein expression in the Ric-8B knockdown cell lines. HEK293T cell lines transfected with control shRNAs (SCR, Scrambled or LUC, luciferase) or with the different shRNAs targeting Ric-8B (shRNA15, shRNA16 and shRNA17) were treated with doxycycline. Total lysates prepared from these cells were analyzed in Western blot experiments for the expression of Ric-8B. Doxycycline (Dox) concentrations used to induce shRNA expression are indicated.

S1 Table. List of all significant downregulated genes in Ric-8B$^{bgeo/bgeo}$ embryos.

S2 Table. List of all significant upregulated genes in Ric-8B$^{bgeo/bgeo}$ embryos.

aCC-BY 4.0 International license.

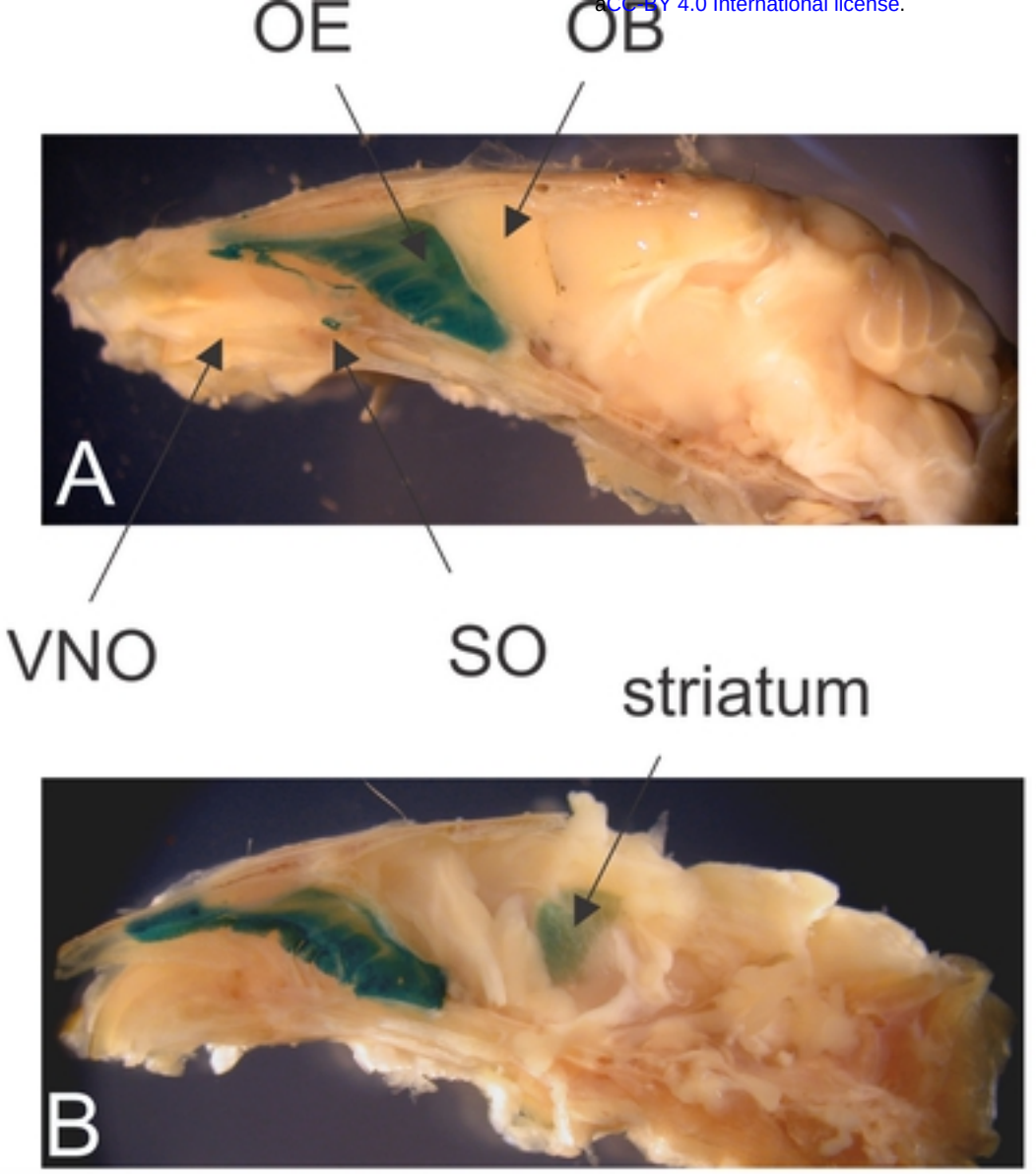

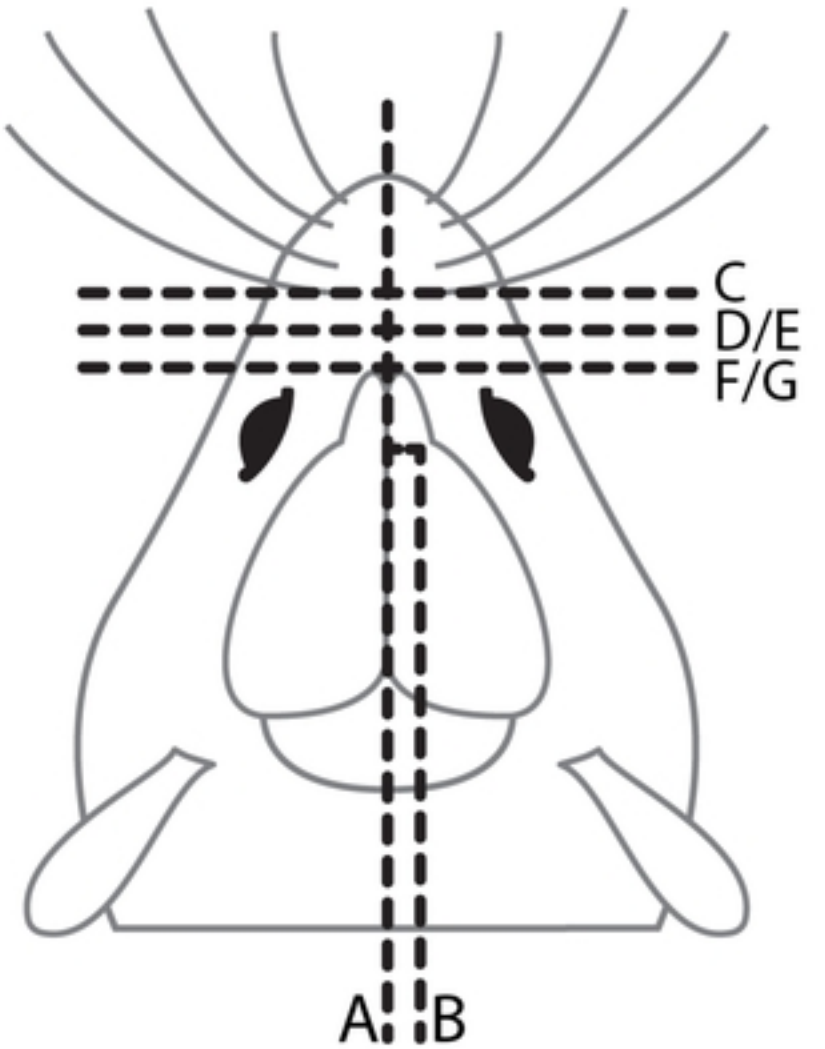

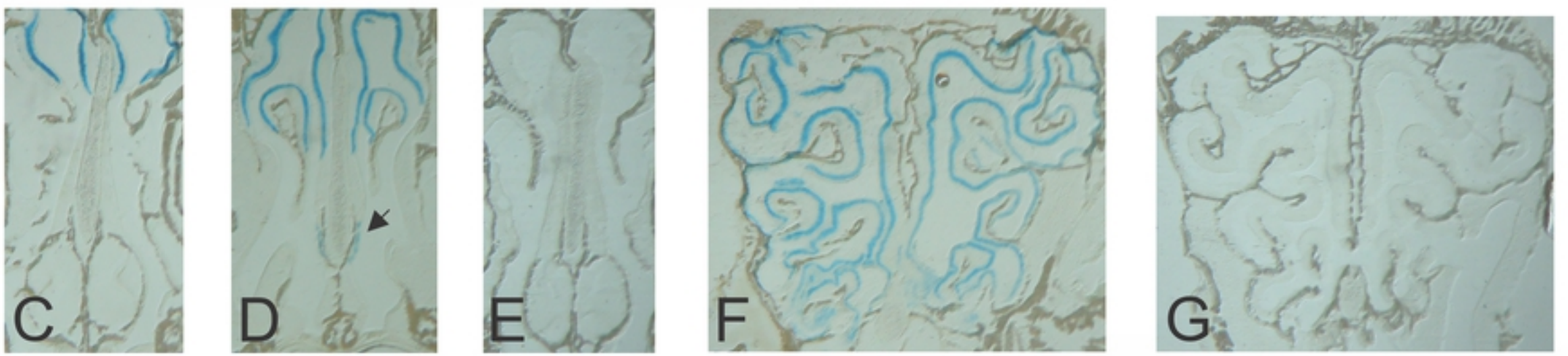

Figure 2

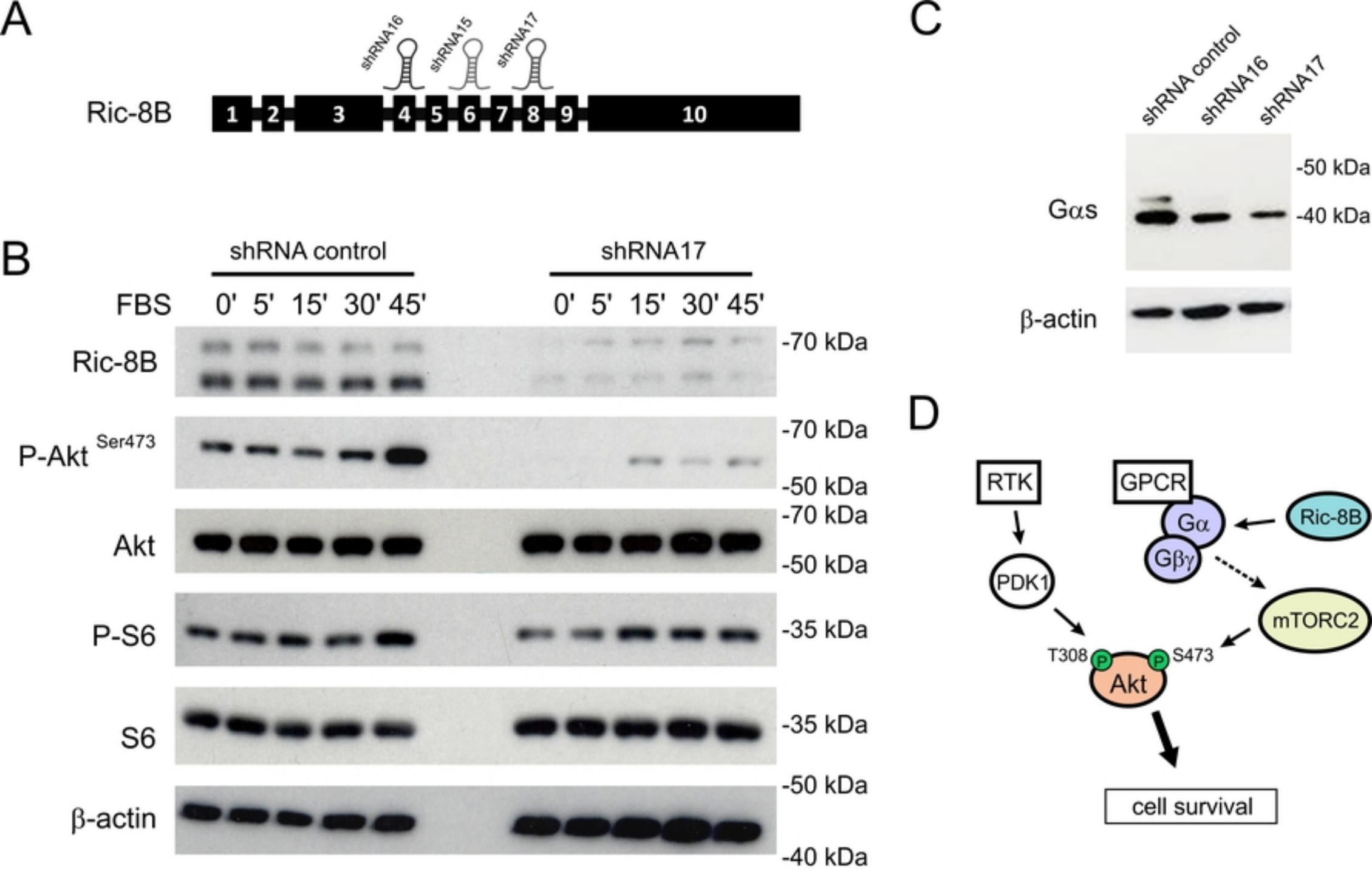
A
shRNA16
shRNA15
shRNA17
Ric-8B
1
2
3
4
5
6
7
8
9
10
B
shRNA control
shRNA17
FBS
0'
5'
15'
30'
45'
0'
5'
15'
30'
45'
Ric-8B
-70 kDa
P-Akt Ser473
-70 kDa
-50 kDa
Akt
-70 kDa
-50 kDa
P-S6
-35 kDa
S6
-35 kDa
β-actin
-50 kDa
-40 kDa
C
shRNA control
shRNA16
shRNA17
Gαs
-50 kDa
-40 kDa
β-actin
D
RTK
GPCR
Gα
Gβγ
Ric-8B
PDK1
mTORC2
T308
P
P
S473
Akt
cell survival

Figure 7

A

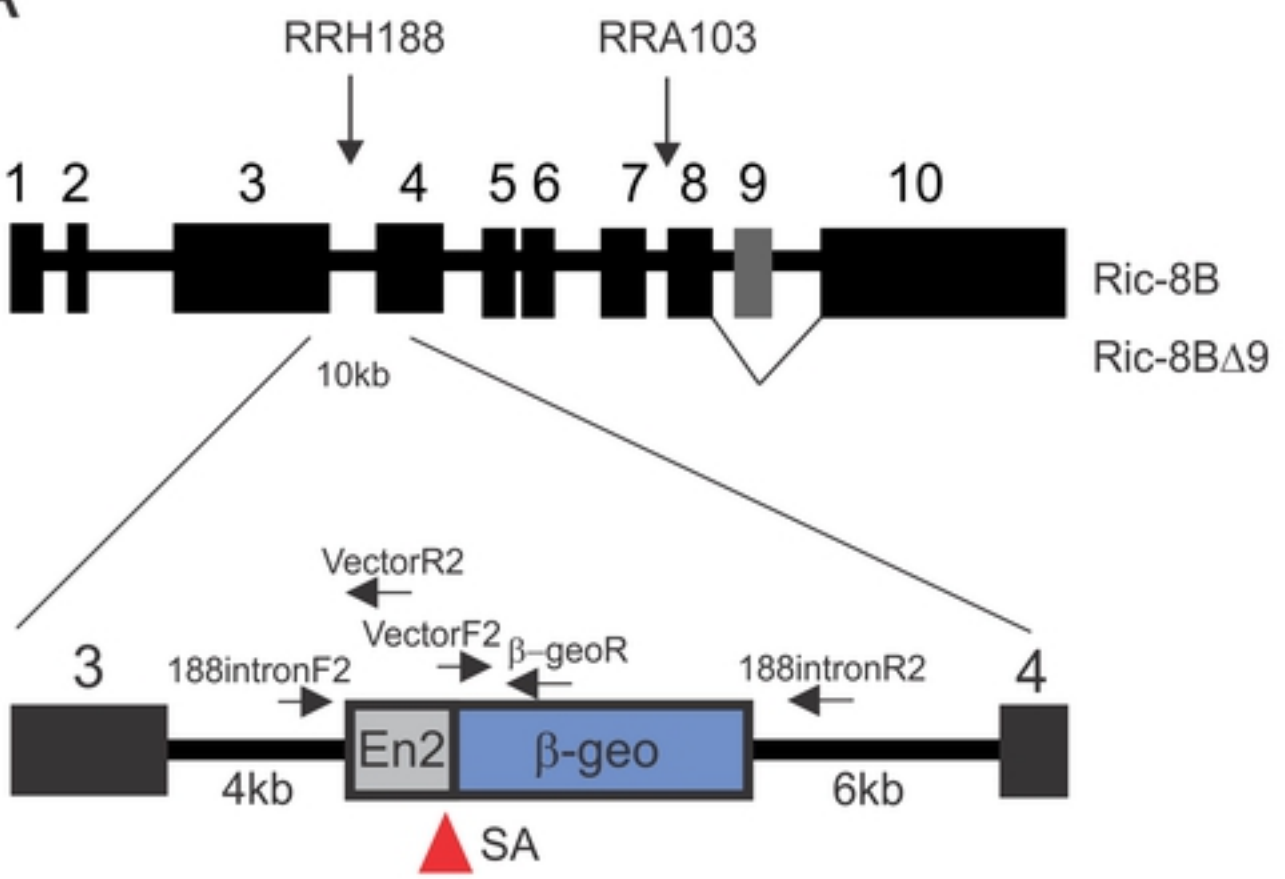

B

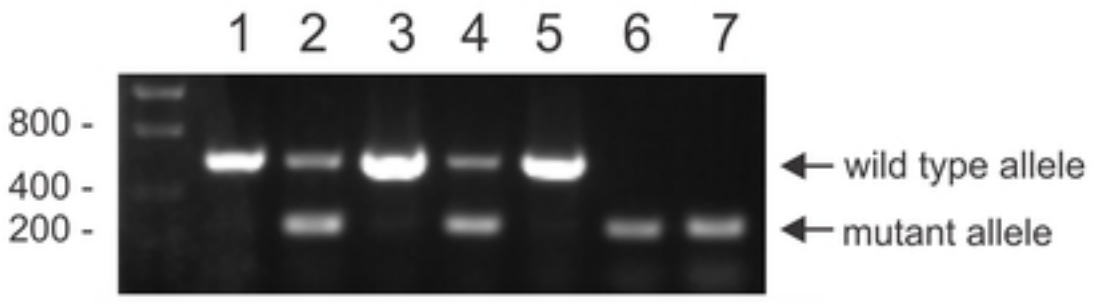

C

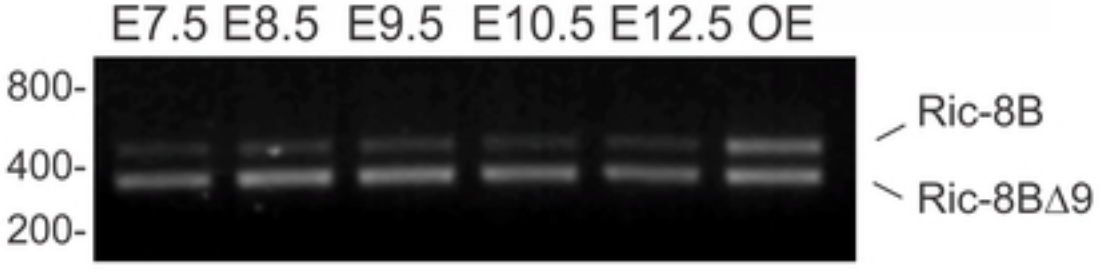

D

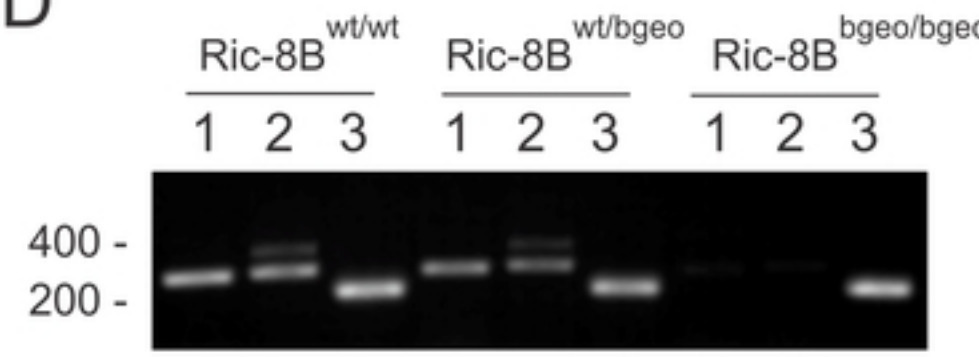

E

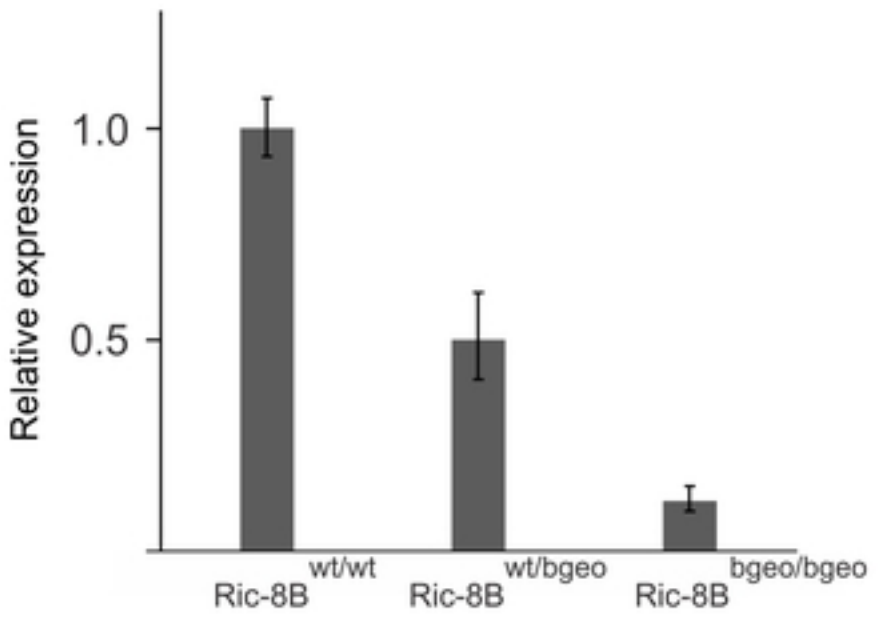

F

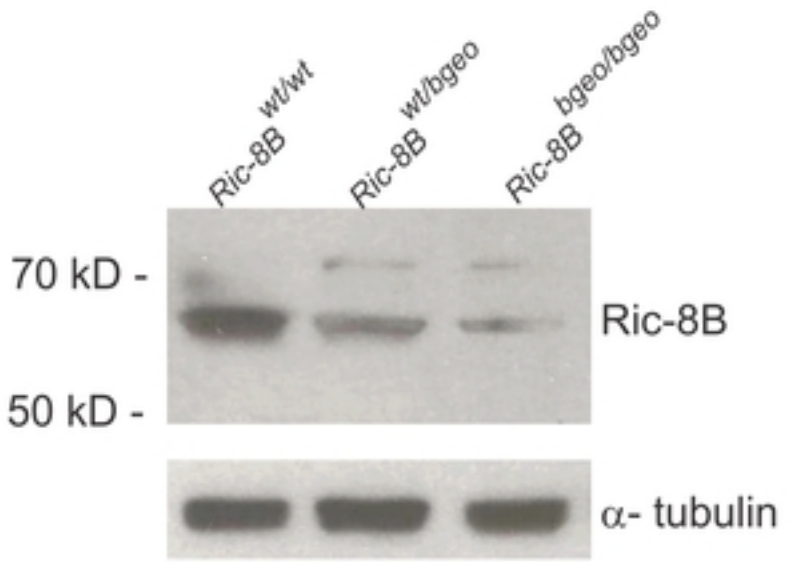

Figure 1

bioRxiv preprint doi: https://doi.org/10.1101/677054; this version posted June 19, 2019. The copyright holder for this preprint (which was not certified by peer review) is the author/funder, who has granted bioRxiv a license to display the preprint in perpetuity. It is made available under aCC-BY 4.0 International license.

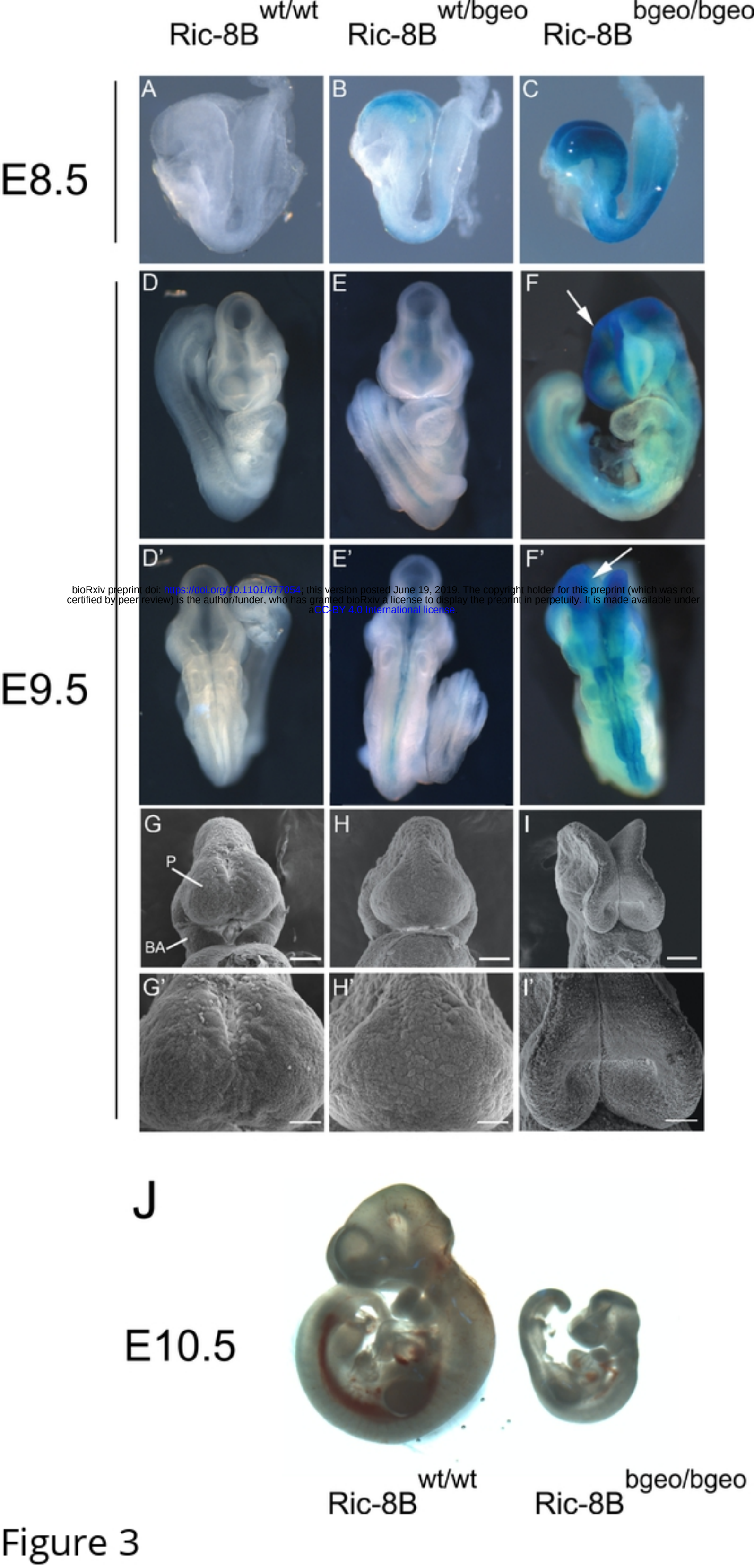

Figure 3

bioRxiv preprint doi: https://doi.org/10.1101/677054; this version posted June 19, 2019. The copyright holder for this preprint (which was not certified by peer review) is the author/funder, who has granted bioRxiv a license to display the preprint in perpetuity. It is made available under aCC-BY 4.0 International license.

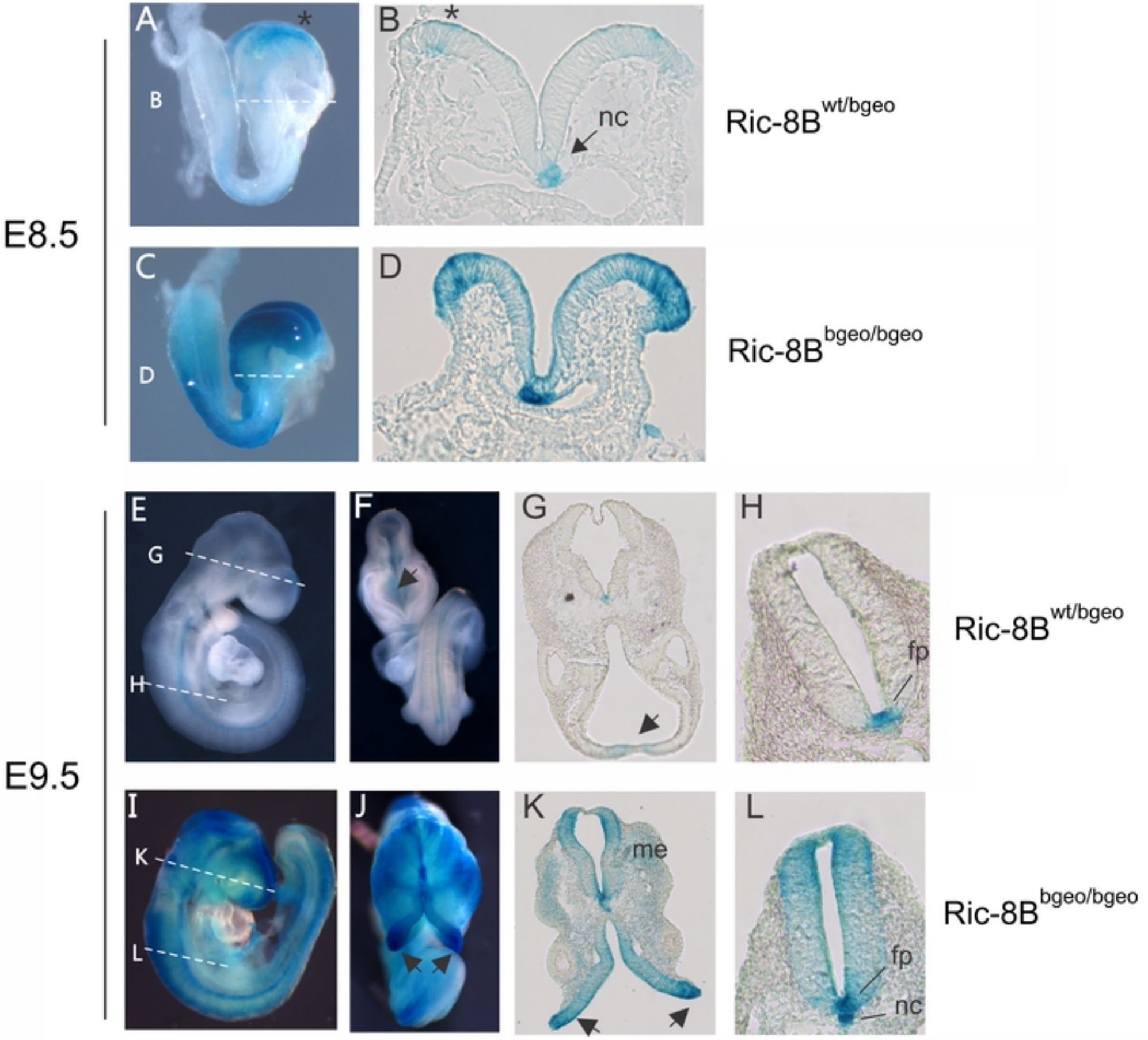

Figure 4

A

Ric-8B$^{wt/wt}$ Ric-8B$^{wt/bgeo}$ Ric-8B$^{bgeo/bgeo}$

F-actin

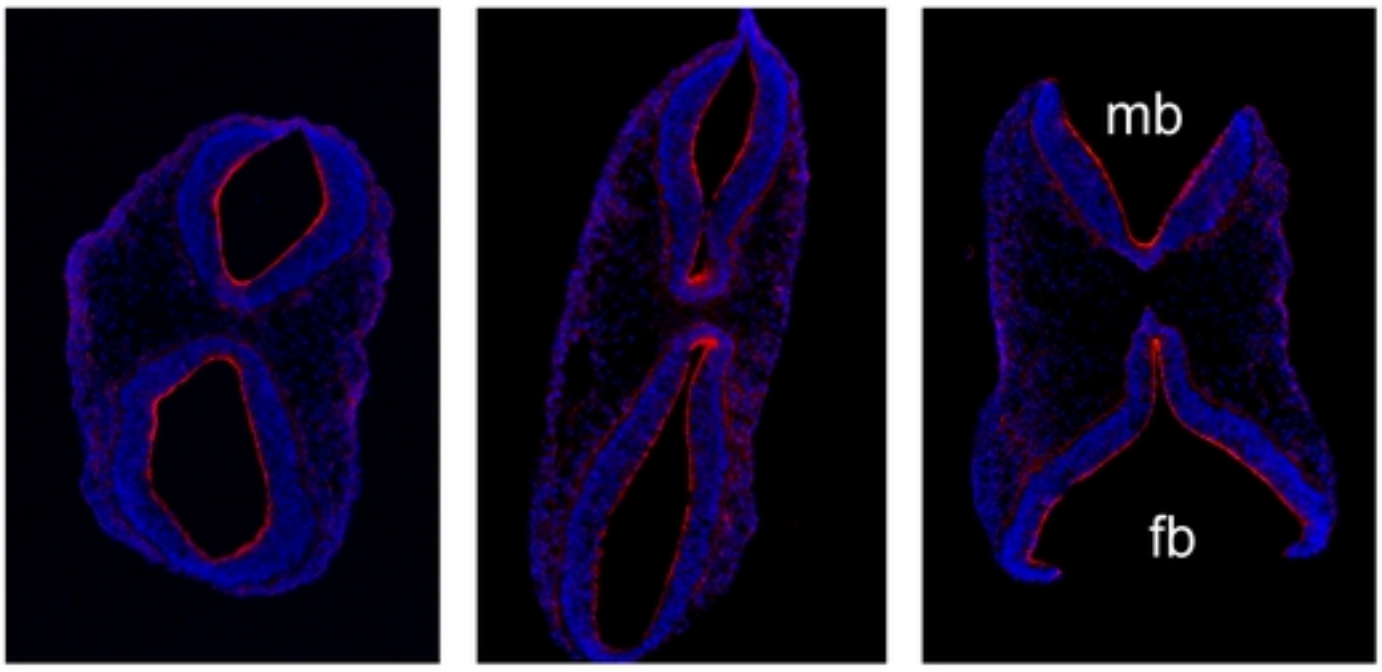

B

Ric-8B$^{wt/wt}$ Ric-8B$^{wt/bgeo}$ Ric-8B$^{bgeo/bgeo}$

activated caspase 3

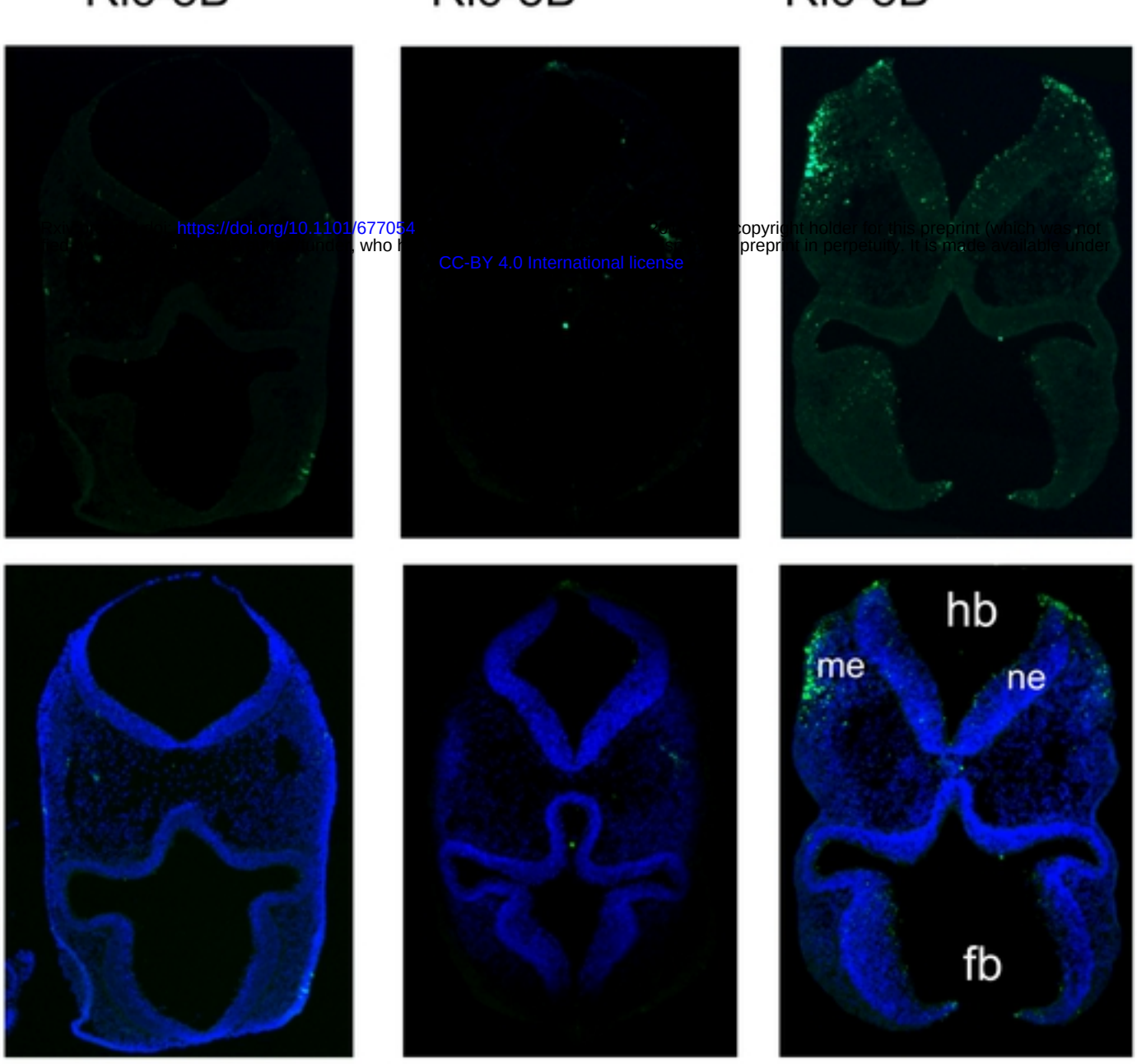

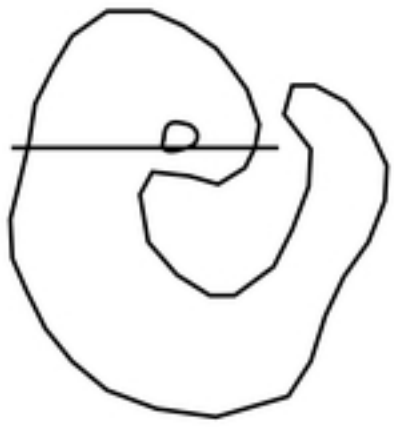

https://doi.org/10.1101/677054
CC-BY 4.0 International license

C

Ric-8B$^{wt/wt}$ Ric-8B$^{bgeo/bgeo}$

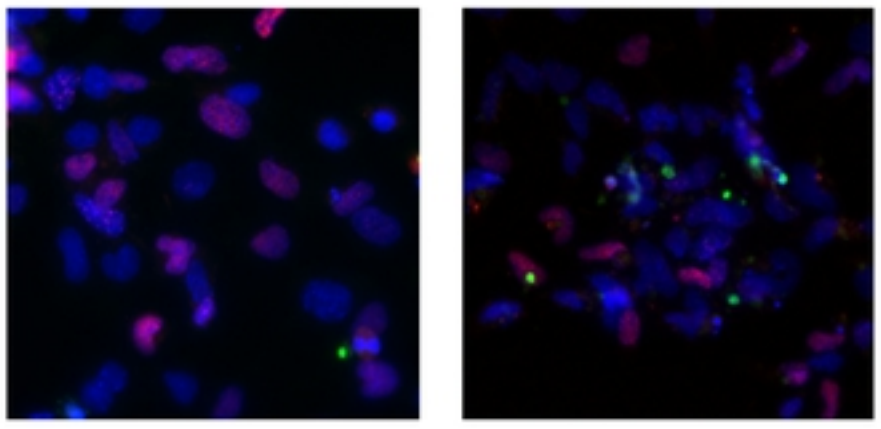

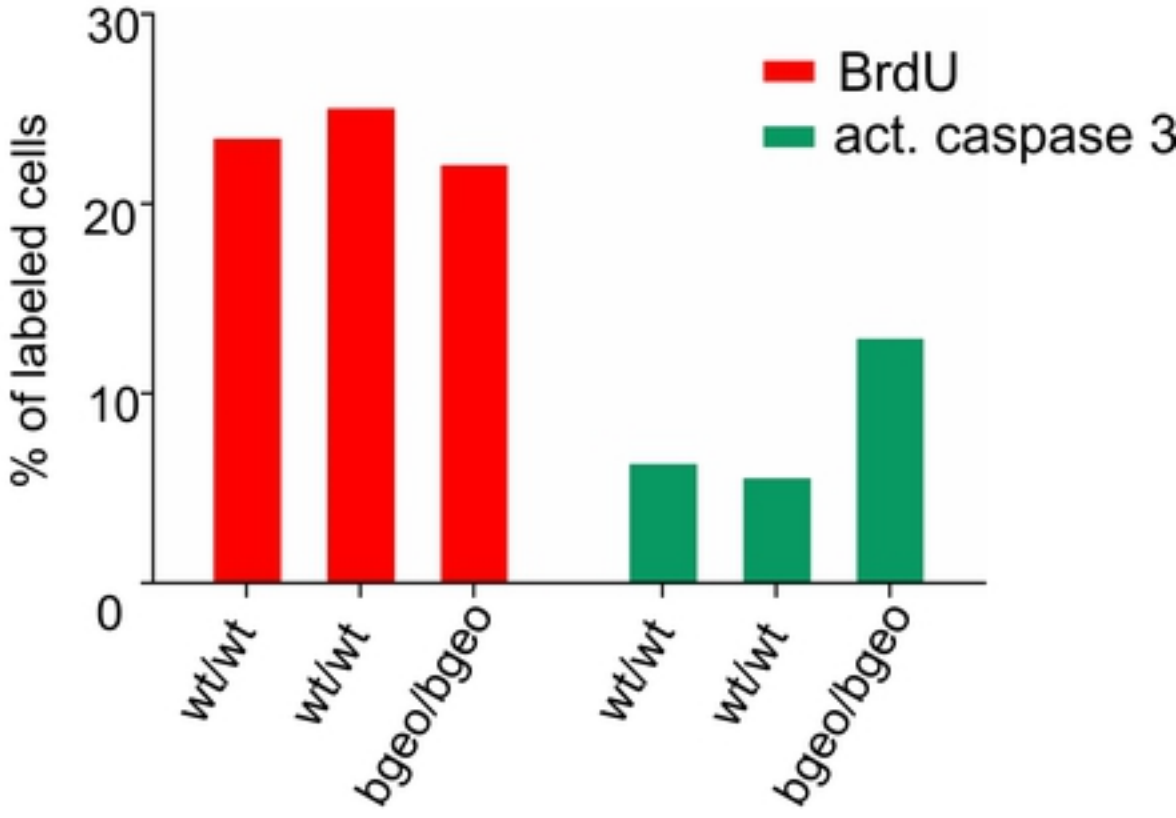

Figure 5

bioRxiv preprint doi: https://doi.org/10.1101/677054; this version posted June 19, 2019. The copyright holder for this preprint (which was not certified by peer review) is the author/funder, who has granted bioRxiv a license to display the preprint in perpetuity. It is made available under aCC-BY 4.0 International license.

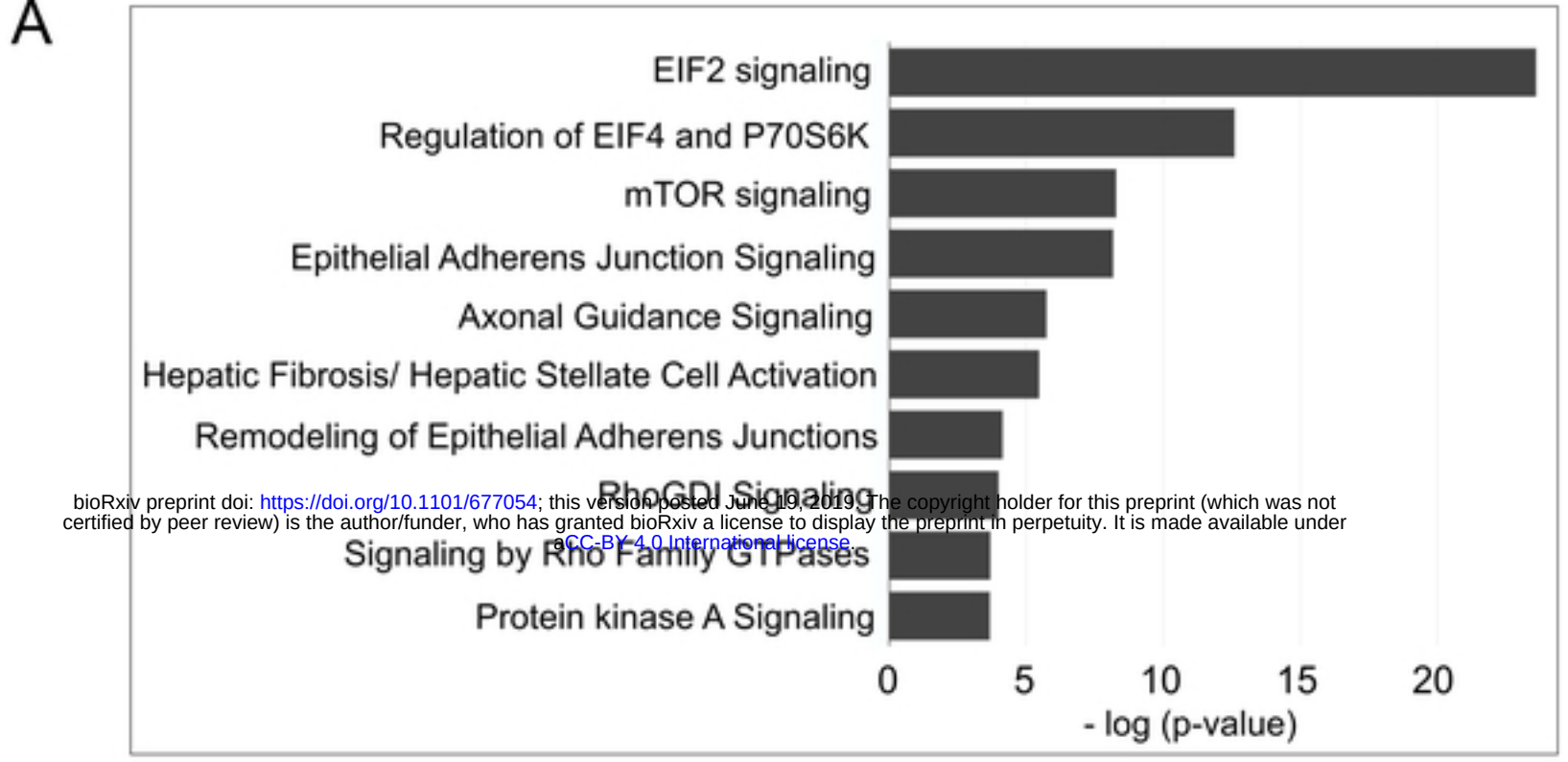

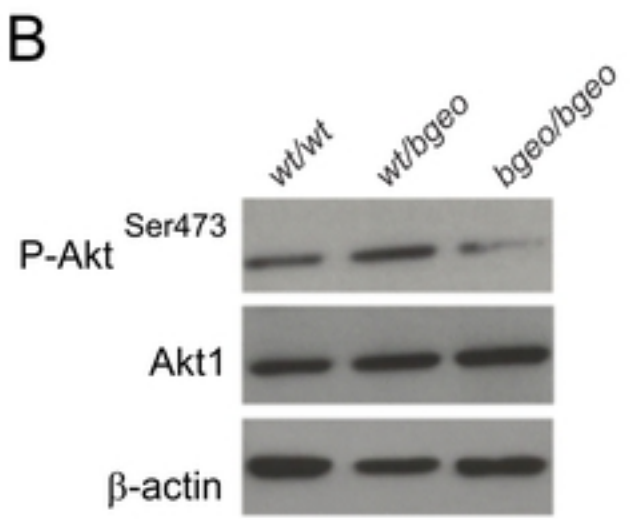

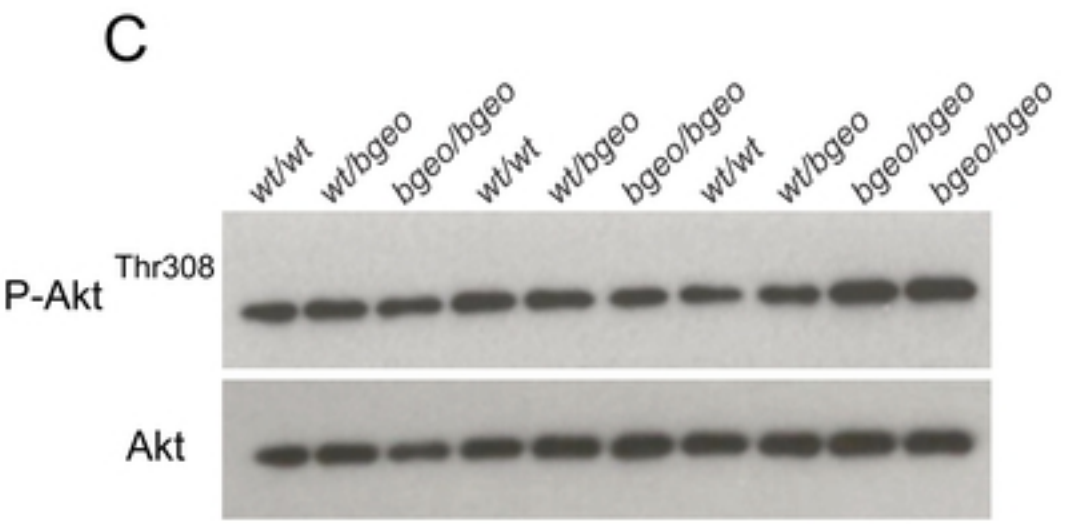

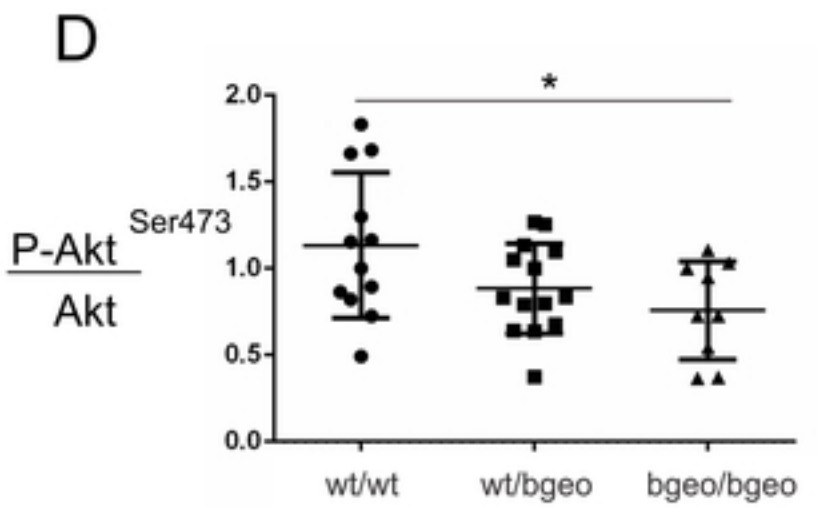

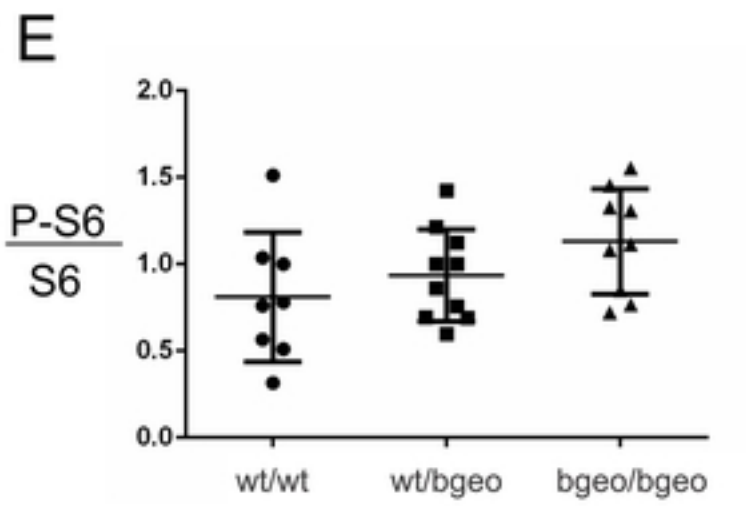

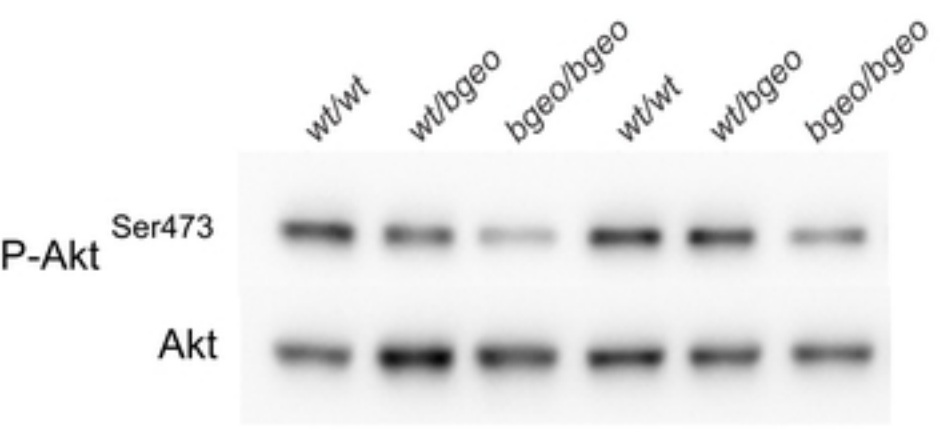

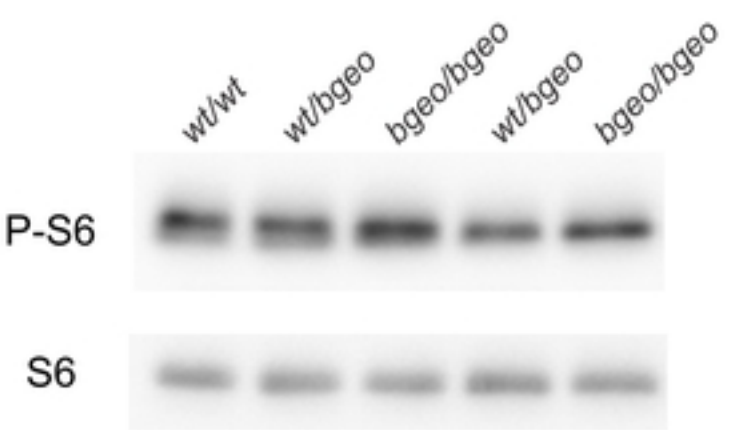

Figure 6